FACULDADE DE ENGENHARIA DA UNIVERSIDADE DO PORTO

Patient-specific FFR quantification implementing and using a 5-element Windkessel model

Diogo Oliveira Freitas

Mestrado em Engenharia Mecânica

Supervisor: Prof. Sónia Isabel Silva Pinto

Co- Supervisor: Prof. Luísa Maria Pimenta Abreu Costa Sousa

April 15, 2022

Patient-specific FFR quantification implementing and using a 5-element Windkessel model

Diogo Oliveira Freitas

Mestrado em Engenharia Mecânica

April 15, 2022

Abstract

Currently, cardiovascular diseases (CVDs) are the leading death cause worldwide. In 2019, an estimated 17.9 million people died of CVDs, which represents 32% of annual global deaths. On top of this, it is also a very common cause of disability, reduced quality of life and economical costs (approximately 372€ per capita in the European Union).

In this work, two patient-specific geometries of the left coronary artery (LCA) were generated in order to perform hemodynamic simulations using computational fluid dynamics, with the objective of calculating the value of the Fractional Flow Reserve (FFR). The computed FFR values obtained were compared with invasively measured FFR obtained by the Vila Nova de Gaia/Espinho Hospital Center (CHVNG/E).

The geometry of the patients' LCA was modeled through computed tomography angiography images that were provided by the CHVNG/E and scaled by a factor of 2.04 of the cross sectional area to represent the patients' geometries under hyperemic conditions of FFR measurement.

In order to properly simulate coronary blood flow, a patient-specific Womersley velocity profile was used as the velocity boundary condition in the inlets. A simplified Phan-Thien/Tanner rheological model was implemented to model blood's viscoelastic properties. Furthermore, a patient-specific five-element Windkessel model was implemented as the pressure boundary condition for the outlets of the models which, to the author's knowledge, hasn't been done while simultaneously using a sPTT model for blood's viscoelastic properties. The Windkessel model is composed of five elements: arterial resistance (R_a), arterial microcirculation resistance ($R_{a,micro}$), venous resistance ($R_v + R_{v,micro}$), arterial compliance (C_a) and intra-myocardial compliance (C_{im}). These elements were estimated in order to produce realistic properties of coronary blood flow. Since the compliances were estimated in relationship to the patient's myocardial mass and this parameter wasn't made available to the author, a sensibility study of the model with changes in this parameter was performed.

Two patients were analyzed in this study. Patient 1 has a 40% stenosed region in the proximal region of the left anterior descending artery and Patient 2 has a 90% stenosis in the medium third of the same artery. The CHVNG/E reported FFR values measured invasively of 0.93 for Patient 1 and 0.59 for Patient 2. A lesion is considered to be in need of intervention for values of $FFR < 0.75$ and hemodynamically irrelevant for values of $FFR > 0.8$. The models implemented for both patients produced FFR values of 0.925 for Patient 1, which corresponds to a relative error of $e_r = 0.53\%$, and a value of 0.719 for Patient 2, corresponding to $e_r = 24\%$. When changing the values of the compliances, virtually no change was detected in the FFR values obtained, which made it clear that the model has very low sensibility to these changes.

From the results obtained, we can see that the model holds up well for arteries with small

lesions, while it lacks in accuracy for more accentuated stenosed areas, due to a inability to accurately represent the patient's geometry under hyperemic conditions.

Keywords: Hemodynamic simulation, Fractional Flow Reserve, left coronary artery, Windkessel model, computational fluid dynamics, stenosis

Acknowledgements / Agradecimentos

Após 5 anos de estudo a nível superior, esta dissertação de mestrado é o culminar de todo o trabalho realizado e conhecimento adquirido ao longo deste tempo. O seu desenvolvimento foi possível, devido a um semestre de trabalho pessoal e também de muitos intervenientes que tornaram possível não só este trabalho como todo o meu percurso académico, alguns dos quais preza-se referenciar.

Gostaria de agradecer à minha orientadora, a Professora Doutora Sónia Isabel Silva Pinto, por ter mostrado todo o seu interesse por este tema, por ter confiado em mim a responsabilidade de o trabalhar e por todo o apoio que me proporcionou durante este semestre de trabalho.

Em segundo lugar, gostaria de agradecer à minha co-orientadora, a Professora Doutora Luísa Maria Pimenta Abreu Costa Sousa, pelo apoio prestado e pelos seus valiosos conselhos.

Gostaria de aproveitar também para agradecer à Fundação para a Ciência e Tecnologia (FCT) pelo financiamento do projeto "Coronary Artery Disease Numerical Simulation and Functional Assessment by Advanced Computed Tomography" - PTDC/EMD-EMD/0980/2020, aprovado em novembro de 2020 e que tornou possível a realização desta dissertação.

Considero também importante deixar o meu profundo agradecimento às instituições envolvidas no projeto e que contribuíram para o seu desenvolvimento: a Faculdade de Engenharia da Universidade do Porto (FEUP) e ao seu Departamento de Engenharia Mecânica (DEMec), o INEGI, a Faculdade de Medicina da Universidade do Porto (FMUP) e o Centro Hospitalar de Vila Nova de Gaia/Espinho (CHVNG/E). Em particular, queria agradecer ao Professor Doutor Nuno Bettencourt, ao Professor Doutor Ricardo Ladeiras-Lopes, ao Dr. Nuno Dias Ferreira e ao Dr. Diogo Ferreira, pelo fornecimento das imagens médicas e pelo recolhimento e disponibilização dos dados sobre os pacientes em estudo.

Não poderia também não deixar uma palavra às pessoas que me apoiaram a nível pessoal e não académico, cuja existência e presença na minha vida ao longo deste tempo foi fulcral para este trabalho. Aos meus pais e à minha irmã, por me terem dado todo o apoio e também confiança para prosseguir com so meus objetivos. Aos meus amigos, por me tornarem uma pessoa mais completa e me ajudarem a ter motivação para continuar a trabalhar e a superar-me. Por último, à minha namorada, por ser também um alicerce de suporte que me permitiu encarar este desafio e preserverar.

Diogo Oliveira Freitas

"The essence of the independent mind lies not in what it thinks, but in how it thinks."

Christopher Hitchens

Contents

List of Figures

List of Tables

Abbreviations and symbols

0.1 Abbreviations

AVs	Atrioventricular Valves
CFD	Computational Fluid Dynamics
CHD	Coronary Heart Disease
CHVNG/E	Vila Nova de Gaia/Espinho Hospital Center
CVD	Cardiovascular Disease
CTA	Computed Tomography Angyography
DBP	Diastolic Blood Pressure
ECG	Exercise Electrocardiogram
FFR	Fractional Flow Reserve
GNFs	Generalized Newtonian Fluids
LAD	Left Anterior Descending Artery
LCA	Left Coronary Artery
LCx	Left Circumflex Artery
RBCs	Red Blood Cells
RCA	Right Coronary Artery
SBP	Systolic Blood Pressure
sPTT	simplyfied Phan-Thien/Tanner model
UFF	User Defined Function
UNCOL	UNiversal COmpiler-oriented Language
WBCs	White Blood Cells
WWW	*World Wide Web*

0.2 Symbols

$\hat{}$	Upper convected derivative
∇	Gradient operator
A	Area $[m^2]$
C	Compliance or capacitance $[m^3/Pa]$
d	Diameter $[m]$
g	Gravity $[m/s^2]$
HR	Heart rate $[bpm]$
I	Identity matrix
i	Imaginary unit
J_0	Zero order Bessel function $[m]$
L	Inductance $[kg/m^4]$
l	Length $[m]$
P_{avg}	Average pressure along the cardiac cycle $[Pa]$
P_{diast}	Diastolic blood pressure $[Pa]$
P_{syst}	Systolic pressure in the aorta $[Pa]$
p	Pressure $[Pa]$
p_{aortic}	Aortic pressure $[Pa]$
p_{distal}	Distal pressure $[Pa]$
Q	Volume flow rate $[m^3/s]$
R	Resistance $[Pa.s/m^3]$
Re	Reynolds number
r	Radius $[m]$
T	Period $[s]$
t	Time $[s]$
V	Magnitude of the velocity $[m/s]$
v	Velocity vector $[m/s]$
Wo	Womersley number
Z	Impedance $[Pa \cdot s/m^3]$

0.3 Greek Symbols

$\dot{\gamma}$	Rate of strain tensor $[s^{-1}]$
λ	Relaxation time $[s]$
η	Dynamic Viscosity
ν	Kinematic Viscosity
ρ	Density
ω	Omega
τ	Viscous Stress

Chapter 1

Introduction

The heart is a vital organ for a person's existence. Currently, cardiovascular diseases (CVDs) are the leading death cause worldwide. In 2019, an estimated 17.9 million people died of CVDs, which represents 32% of annual global deaths [26]. On top of this, it is also a very common cause of disability, reduced quality of life and economical costs (approximately 372€ per capita in the European Union). Their risk factors are nevertheless well reported, the main being tobacco use, raised blood pressure and high blood cholesterol. [14]

Coronary heart disease (CHD) represents approximately one third to one half of total CVD cases and is the cause of approximately one third of all deaths in developed countries [16]. Its origin is routed in the development of coronary atherosclerosis [30], a chronic and progressive disease which consists on the accumulation of lipids and fibrous elements in medium-sized and large arteries [10]. This accumulation can lead to a luminal narrowing of the arteries, called stenosis, which may lead to reduced blood flow and an imbalance between oxygen supply and demand in the myocardium. The described imbalance is what characterizes CHD and can eventually lead to a heart attack. Such dangers to one's well being leads to a necessity in treatment, consisting overall in proper medication, lifestyle changes, and revascularization when needed [18].

Since revascularization can lead patients to problematic side effects, it is of utmost importance that one can determine if a stenosis leads to ischemia and the need of revascularization [13]. When a patient's stenosis is large enough, ischemia might be diagnosed by non-invasive methods such as the analysis of images obtained with computed tomography angiography (CTA) or exercise electrocardiogram (ECG). For patients with intermediate-grade stenosis, this sort of evaluation often isn't able to identify the occurrence of ischemia. In these situations, the standard for the functional assessment of the severity of a lesion is the fractional flow reserve (FFR), which is the ratio between maximum myocardial flow in a stenotic artery and the same flow if the artery was healthy and represents the extent to which myocardial blood flow is limited by the presence of the stenosis [11] [45].

The current standard procedure to determine the value of FFR consists on inserting a wire in

the artery where the stenosis is located, while on hyperemic conditions, and measuring the aortic pressure and the pressure distal to the lesion [12]. In alternative, research has increasingly been made in the use of computational fluid dynamics (CFD), coupled with CTA, for obtaining FFR values by solving the governing equations of fluid dynamics for coronary blood flow. These CFD simulations, apart from the governing equations, need to have a domain of simulation specified and boundary conditions for each of its boundaries, which will impact the accuracy of the results obtained [5].

Following promising results from the usage of a three-element Windkessel model, in this work, a five-element Windkessel model will be applied as the boundary condition for the pressure in the outlets of pacient-specific left-coronary artery (LCA) models under hyperemic conditions, during CFD simulations of the blood flow [3]. The results of these simulations will then be used to determine the FFR values of each patient and compare them to the invasive FFR measured invasively at the Vila Nova de Gaia/Espinho Hospital Center (CHVNG/E).

1.1 Motivation

With the rising interest in hemodynamic CFD simulations, there have been researchers experimenting with different boundary conditions. The five-element Windkessel model as been therefore studied for application in the outlets of LCA models. Nevertheless, there hasn't been investigation combining this boundary condition with the viscoelastic properties of blood.

This work will elaborate on the promising results shown in the usage and implementation of a five-element Windkessel model for the LCA outlet's, coupled with a simplyfied Phan-Thien/Tanner model (sPTT) developed by Pinto et al. [32] to describe blood's rheology. With the usage of a five-element Windkessel model, it is expected that the FFR values obtained will gain accuracy, due to a more accurate representation of the pressure distribution across the LCA [3].

The main motivation of this work is to produce a model that can accurately reproduce the LCA's hemodynamics and therefore properly predict the appearance of ischemia. This is an important contribution to the development of a non-invasive and safe way to obtain the FFR value of a stenosis, which to the authors knowledge is still not possible.

1.2 Objectives

This dissertation has the main objective of calculating the FFR value of patients' stenosis, through the usage of pacient-specific models of their LCA, and compare the results to the FFR obtained through an invasive method. To meet this goal, the steps that are next described were followed.

First, it was necessary to obtain a 3D model of the patients' LCA. This was done by reconstructing the lumen from CTA images and then altering it to be scaled in the hyperemic conditions in which the FFR was measured, utilizing the software Mimics® to obtain the 3D model from the CTA images and the software 3-matic® to modify the model into desired conditions.

The obtained LCA models were then used in ANSYS Fluent® to simulate the coronary blood flow. In this software, the five-element Windkessel model was implemented and loaded as the boundary condition for the pressure in the outlets using a user-defined function (UDF). The hemodynamic properties of each patient differ and so did the parameters used in the lumped-parameters model of the UDF.

The results were then compared to the FFR obtained by medical invasive measurement in order to better adjust the parameters of the Windkessel model and produce the most accurate results possible.

1.3 Structure of the dissertation

This dissertation is organized into eight chapters. In chapter 2, the cardiovascular system is reviewed. The cardiac cycle is described and general characteristics of blood's circulation are presented, as well as the characteristics of atherosclerosis and the standard measurement procedures for FFR.

In chapter 3, some basic concepts of fluid mechanics are discussed, in order to lay the foundations for the hemodynamic simulations in which this work is based on.

In chapter 4, blood's rheological behaviour is reviewed and thus its viscoelastic properties are presented, which helps understand blood flow phenomenon.

In chapter 5, the fundamental principles of modeling coronary blood flow are described. Then, it is presented how the electrical circuit analogy is utilized to develop lumped-parameters models that can condense the principal characteristics of blood flow.

In chapter 6, the methodology that this work followed is presented.

In chapter 7, the results obtained are analyzed and discussed, with the review of the FFR values obtained through the computational method developed and a comparison to the ones obtained through invasive measurement.

In chapter 8, the main conclusions of this work are outlined, as well as some suggestions for possible further works on the area being presented.

Chapter 2

Cardiovascular System

As human beings, we remain alive due to very complex control systems, one of which is the cardiovascular system. Circulation of blood is considered the transport system that serves the needs of internal organs of the body of all mammals. The circulation through the various organs is done through the blood vessels and performs various transport functions, the major substances transported being oxygen, carbon dioxide and nutrients [25].

Blood leaves the heart and is transported by pressure differential to the capillaries by the arteries and is then returned to the heart by the veins. Since pressure in the arteries is much higher, their walls are also much thicker than that of the veins. The capillaries are the smallest blood vessels and, because of being thin and porous, have the function of exchanging fluid, nutrients, electrolytes, hormones and other substances between blood and interstitial fluid[1] [16] [25] [4].

The circulatory system consists of the heart, the lymphatic system (which transports solutes and fluids that are diffused from the fluid that surrounds the cells back to the blood), the pulmonary circulation and the systemic circulation.

2.1 The human heart

The heart is a muscular organ located in the middle mediastinum, between the lungs, lying in the protective torax and resting in the superior surface of the diaphragm. It's main function is to pump blood thought the circulatory system [42] [16].

2.1.1 Anatomy

The human heart, represented in figure 2.1, is composed of two ventricles and two atria, separated by the interatrial septrum, which connect the pulmonary circulation with the systemic circulation. The atria are located in the upper part of the heart and work as collecting chambers, while the ventricles are located in the bottom part and are much stronger, having the function of pumping

[1] Fluid found in spaces between the cells

blood [39]. Surrounding the heart there is a two-layer sac called the pericardium, which protects and holds the heart in position [16].

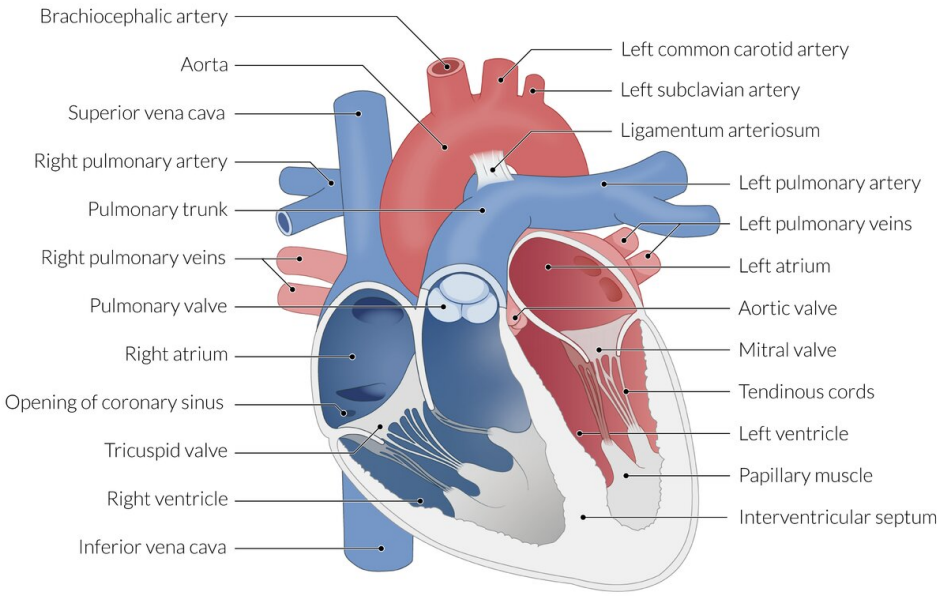

Figure 2.1: Heart Anatomy. Adapted from [2]

2.1.2 The Heart as a Pump

In terms of it's functionality, the heart can be divided into two separate pumps, the right part which pumps blood through the lungs and the left heart that pumps it through the systemic circulation [16].

Each part is composed of an atrium and a ventricle. The atrium receives blood and proceeds to deliver it to the corresponding ventricle, serving as a minor pump that initiates blood circulation. The ventricles, much stronger pumps, serve as the main pumping force, that propel the blood out of the heart and into each circulation system [16].

- The right atrium receives deoxygenated blood from the superior vena cava, inferior vena cava and the coronary veins and pumps it into the right ventricle.
- The left atrium receives oxygenated blood from the pulmonary veins and pumps it into the left ventricle.
- The right ventricle receives blood from the right atrium and pumps it out of the heart into the pulmonary trunk, initiating the pulmonary circulation.

- The left ventricle receives blood from the left atrium and pumps it into the aorta, initiating the systemic circulation [2].

Connecting the ventricles to the atrium are the atrioventricular valves (AVs), which close and open by the pressure differential between the atrium and respective ventricles, preventing back-flow in blood circulation. The outlets of the left and right ventricles are home to the aortic and pulmonary valves, which close when the pressure inside the ventricles is high and open in order to let the blood be pumped out when the ventricles relax [16] [2].

2.1.3 Cardiac Cycle

The heart works in a cyclic manner, with a repetitive list of actions that occur cyclically from the beginning of a heartbeat until the beginning of the next. This sequence is called cardiac cycle. Each cardiac cycle is initialized by an action potential in the sinus node, which is located in the superior lateral wall of the right atrium, next to the outlet of the superior vena cava [16]. Figure 2.2 represents the evolution of pressure and volume of both atrium and ventricles through the cycle.

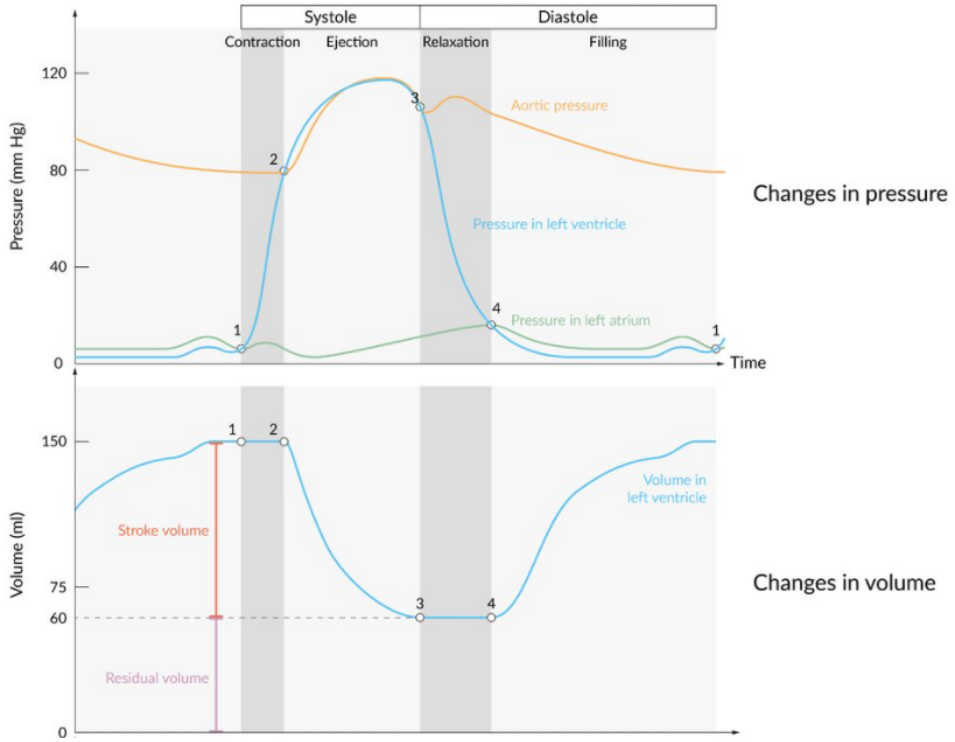

Figure 2.2: Evolution of volume and pressure across the cardiac cycle. Adapted from [1]

This cycle can be divided into two major parts, the systole, where the blood is pumped to the outside, and the diastole, in which the heart is filled with blood. These two phases can be divided into two further phases, which makes the cardiac cycle divided into four different actions, the first two corresponding to the systole and the latter to the diastole [1]:

- Isovolumetric contraction (1-2 in figure 2.2): the AVs close (all valves are closed) and ventricular pressure increases while the ventricle's volume is constant.
- Systolic ejection (2-3 in figure 2.2): the aortic and pulmonary valves open, ventricular volume decreases as its pressure increases and blood is pumped into the circulatory systems.
- Isovolumetric relaxation (3-4 in figure 2.2): both the aortic and pulmonary valves close and the pressure in the ventricles decreases without a change in their volume, until it is lower than artrial pressure which causes the AVs to open.
- Ventricular filling (4-1 in figure 2.2): corresponds to the transport of blood from the atrium to the ventricles, which is done by the opening of the AVs and is done initially at a high pace that decreases until the end of the diastole [1] [16].

2.2 Blood circulation

As discussed earlier, blood transport can be divided into two different systems, which are connected by the heart. The vascular network of the human body, through which blood flows, is represented in figure 2.3.

In the pulmonary circulation, deoxygenated blood leaves the right ventricle through a large vessel, the pulmonary artery (trunk), which shortly divides itself into two arteries, providing blood to the right and left lungs [39]. The blood from both arteries is carried to the alveolar capillaries where the gas exchange occurs, oxygen is added and carbon dioxide is removed. Oxygen is then carried with the blood back to the heart, entering the left atrium through the pulmonary veins [16].

The systemic circulation is composed of a similar system. Oxygenated blood is pumped from the left ventricle through the aorta (the largest artery in the human body), which is then divided into progressively slimmer vessels. Blood is propelled through the vessels until arriving at the capillary bed, where it will feed oxygen, water, nutrients and other needed substances to the organs' tissues. After this, blood is returned to the right atrium by the veins [39][16] [4]. This circuit also includes the coronary circulation, which will be analyzed in the next section of this work.

2.2.1 Coronary Circulation

The heart is the human organ with the highest consumption of oxygen per tissue mass [33]. To sustain this elevated need of oxygen as well as of nutrients, the heart has its own delivery system of blood to the tissue, which is the coronary circulation, represented in figure 2.4 [39]. This system is composed of two main arteries that branch from the aorta, the left coronary artery (LCA) and the right coronary (RCA), in which approximately 5% of total blood output from the heart flows, and that feed the heart with almost all of its blood supply, being that only a residual amount of tissue receives it from blood inside the heart's chambers [16] [33] [39]. The LCA supplies mainly the anterior and left lateral parts of the left ventricle and the RCA supplies most of the right ventricle, as well as the posterior part of the left ventricle in right-dominant people (80% to 90%). Both

of the arteries returns most of their blood flow to the right atrium, the LCA through the coronary sinus and the RCA through the anterior cardiac veins [16].

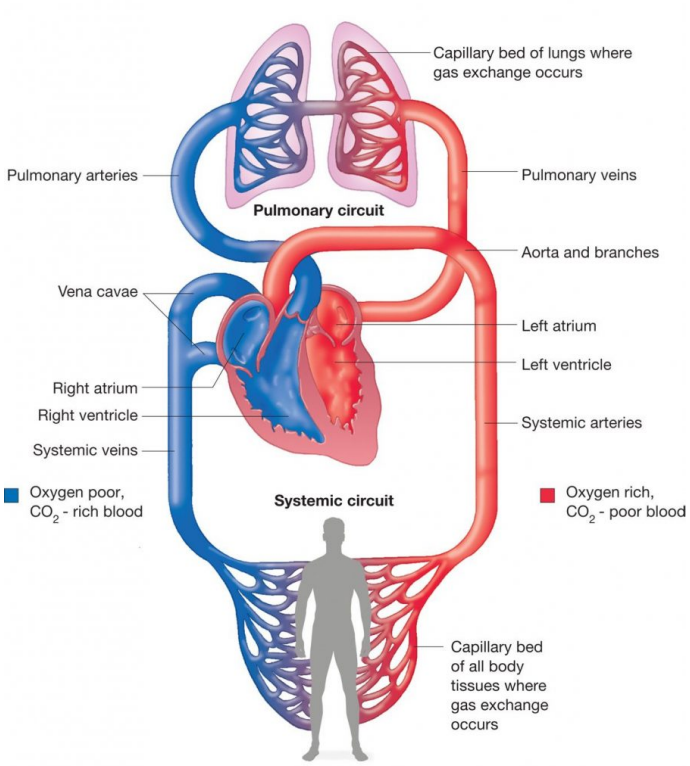

Figure 2.3: Circulatory System. Adapted from [15]

2.3 Left Coronary Artery

The LCA is the biggest coronary artery in diameter, with its main initial portion dividing itself into multiple branches, of which the most important are the left anterior descending artery (LAD) and the left circumflex artery (LCx) [42] [2].

The LAD is considered the continuation of the initial artery, which descends obliquely to the front and left in the anterior interventricular sulcus[2] between the right and left ventricles and gives off several diagonal branches on its course [42]. This artery is a crucial part of the cardiovascular system, with its disease being associated with high mortality and mobility issues due to it feeding a large area of myocardium tissue [25]. The grave consequences of LAD disease, specially LAD infarction[3], have even led to it being given the nickname "widow maker" [2].

The LCx has a diameter that is similar to the LAD. It curves to the left in the interventricular sulcus, developing through the left margin of the heart in the posterior part of the sulcus and ending

[2] groove that separates the heart's ventricles
[3] tissue death due to insufficient blood supply

before the posterior interventricular sulcus. Through its path, the LCx branches into left marginal arteries [42] [2].

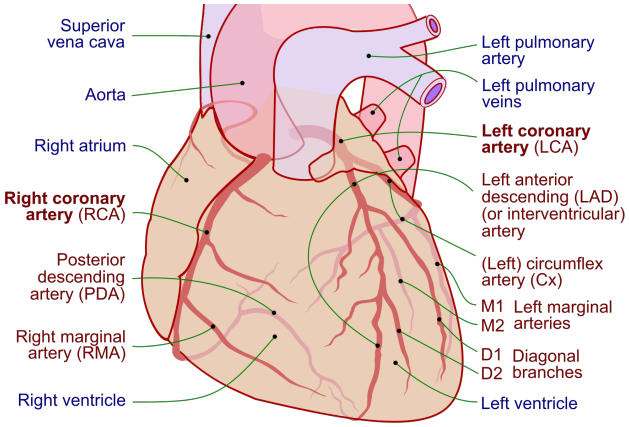

Figure 2.4: Coronary circulation. Adapted from [15]

2.4 Atherosclerosis

Coronary heart disease (CHD) represents approximately one third to one half of total CVD cases and is the cause of approximately one third of all deaths in developed countries [16]. It is caused by the development of coronary atherosclerosis [30], a chronic and progressive disease which consists on the accumulation of lipids and fibrous elements in medium-sized and large arteries [10]. This accumulation can lead to a luminal narrowing of the arteries, called stenosis, which may lead to reduced blood flow and an imbalance between oxygen supply and demand in the myocardium.

The objective of this work is to computationally conclude if the artery of a patient has a severe enough lesion to make it need revascularization.

2.4.1 Fractional Flow Reserve (FFR)

In order to describe the severity of a stenosis, the gold standard for clinical practice is the fractional flow reserve (FFR). This parameter helps one understand if the artery is in need of revascularization or not, being shown to reduce unnecessary interventions and healthcare costs in general, when compared to the other standard procedures.

Despite this, it is still only used for a very small portion of potentially ill patients, due to requiring an invasive procedure, which can be hazardous for the patients' health. Its measuring process consist of inserting a pressure wire into the coronary vessel, under maximum hyperemia conditions, and measuring the value of aortic and distal pressures, p_{aortic} and p_{distal}. The aortic pressure is measured at a distance of $10mm$ from the entrance of the coronary tree, while the distal pressure is measured at a distance of $20mm$ from the stenosed region [45].

A stenosis is considered significant if $FFR < 0.75$, and is considered to be of negligible effect if $FFR > 0.8$. For intermediate values, the clinician is responsible to evaluate if a revascularization could be beneficial or not.

In order to generalize the use of this method, it is of upmost importance that it is made available through a non-invasive method that has no implications for the patient's health. The computational calculus of FFR is thus a promising alternative that intends to optimize this clinical practice [45] [12].

Chapter 3

Hemodynamics

As a fluid, blood's circulation through the circulatory system abides by the rules of fluid mechanics. Flow can be seen as of statistical or continuum nature, depending on if we analyze its microscopic or macroscopic behaviour [27].

Fluid mechanics is usually concerned with blood's macroscopic behaviour, averaging the flow and properties of each cell by groups that surround certain points in space by a small distance, which are called fluid particles. Though small, this distance is large when compared to the distance between cells which, combined with the utilization of time scales much larger than that of molecular vibrations, make it possible to analyse the fluid as a continuum matter[27][41][23].

Thus, we can apply the laws of continuum mechanics to blood flow through the cardiovascular system's vessels. The branch of fluid mechanics that studies such flows is hemodynamics, which will be analyzed in this chapter.

3.1 Properties of the Continuum Fluid

The state of matter can be divided into fluid and solid. The two can be defined by the reaction each has to a tangential (shear) stress. While a solid can resist shear stress by static deformation, a fluid is a substance that deforms continuously when a shear stress of any magnitude is applied[23][41]. In order to understand a fluids behaviour, two properties which identification is key are its density and viscosity.

3.1.1 Density

A fluid's density, denoted by the Greek symbol rho (ρ), is defined as its mass per unit of volume and is usually used to characterize the mass of a fluid [23].

$$\rho = \frac{m}{V} \tag{3.1}$$

It is a function of static pressure, temperature and molecular weight [27]. For a category of fluids called incompressible, ρ is independent of the pressure, while for compressible ones a change in pressure can provoke a change in the fluid's density. To an extent, all fluids are compressible, but one must evaluate the pressure variations that are present in each situation to identify if the fluid can be considered incompressible for such values[41][27].

3.1.2 Viscosity

The relationship between the deformation rate of a fluid and the shear stress that was in its origin is described by its viscosity.

The stress that is applied to an incompressible fluid is represented by a stress tensor, T, which can be divided into an isotropic component due to static pressure, $-pI$, and an anisotropic viscous stress component that is related to the relative motion of fluid particles, τ [27]:

$$T = -pI + \tau \tag{3.2}$$

where I is the identity matrix. This tensor can also be presented through matrices, identifying each component in the Cartesian coordinate system, which is represented in figure 3.1 and will be utilized throughout this section:

$$\begin{pmatrix} T_{xx} & T_{xy} & T_{xz} \\ T_{yx} & T_{yy} & T_{yz} \\ T_{zx} & T_{zy} & T_{zz} \end{pmatrix} = -p \times \begin{pmatrix} 1 & 0 & 0 \\ 0 & 1 & 0 \\ 0 & 0 & 1 \end{pmatrix} + \begin{pmatrix} \tau_{xx} & \tau_{xy} & \tau_{xz} \\ \tau_{yx} & \tau_{yy} & \tau_{yz} \\ \tau_{zx} & \tau_{zy} & \tau_{zz} \end{pmatrix} \tag{3.3}$$

For a fluid with relative motion between particles, one can characterize the rate of strain motion by the rate-of-strain tensor, D:

$$D = \frac{1}{2}[\nabla u + (\nabla u)^T] \tag{3.4}$$

where ∇ is the gradient operator, described by the following vector:

$$\nabla = \left(\frac{\partial}{\partial x}, \frac{\partial}{\partial y}, \frac{\partial}{\partial z} \right) \tag{3.5}$$

and u is the velocity vector.

In this chapter, we will be analyzing flow of Newtonian fluids, which present the following relationship between the two tensors described above [27]:

$$\tau = 2\eta D \tag{3.6}$$

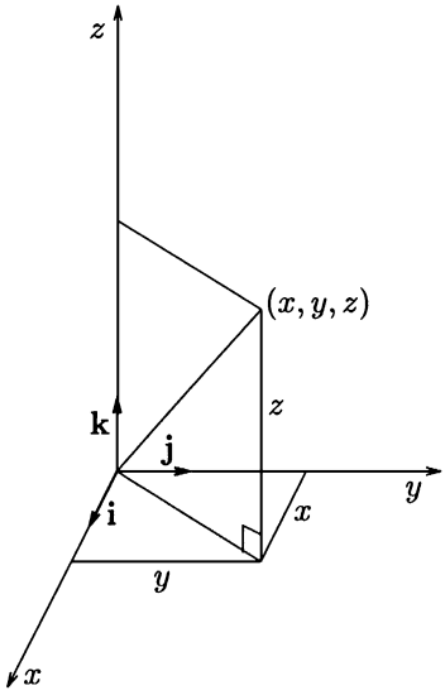

Figure 3.1: Cartesian system of coordinates. Adapted from [41]

where η is the dynamic viscosity of the fluid, which only varies with temperature changes, relating the stress and thee rate of deformation.

The different types of fluids in terms of their viscosity are discussed in the next chapter, where fluids that don't follow equation 3.6 are analyzed.

3.2 Governing equations of steady fluid flow

Having a fluid's parameters been identified, in order to analyze its flow, one must obtain its governing equations and solve them. There are two ways of analyzing fluid flow, the Eulerian Method and the Lagrangian Method.

The latter method consists on following individual fluid particles as they flow and identifying the fluid's properties in such particles as a function of time. The former, which is the most commonly used and the one this work will adopt, consists of analysing specific points in space and the properties of the fluid particles that flow through them in each instant [23].

All mechanical laws are written for systems, which are portions of mass and therefore consist of a Lagragian Method of analysing matter. In order to analyze flow through an Eulerian lens, we must convert the conservation laws that characterize matter movement and apply them to a control volume [41].

Control volumes are arbitrary portions of space, either static or mobile, with open boundaries through which we can analyse the flow entering and leaving and make balances to obtain the changes in properties of the fluid inside the volume. If the control volume used is reduced to an

infinitesimal element, one can obtain quantities to a point-level and thus, obtain the infinitesimal or differential conservation equations, which characterize fluid flow in all of its domain [23] [41].

3.2.1 Reynolds Number

The Reynolds Number is, generally speaking, the first parameter one should obtain when studying a specific flow. It makes use of both fluid's density and viscosity, being the ratio between the magnitudes of inertial and viscous forces [41]:

$$Re = \frac{\rho V L}{\eta} \tag{3.7}$$

L is the flow's characteristic length and V is its average velocity magnitude.

Representing the ratio described above, it follows that for very small Re values, viscous effects are predominant and inertial effects can be neglected, while the opposite happens for high values [41][23].

This parameter lets us separate flows into three categories. For very small values of Re, we have creeping flows. For moderate values, flow is laminar, being characterized by parallel sliding of adjacent fluid layers without the phenomenon of intermixing. Re values higher than a critical point, which varies from case to case (for flow through a pipe it is 2100), the flow starts becoming turbulent, with the formation of eddies that lead to intermixing and an oscillatory chaotic behavior of fluid motion[41].

3.2.2 Conservation of mass

The conservation of mass law dictates that the rate of increase of fluid mass within a control volume is equal to the net influx of fluid across its boundaries. This law is described by the continuity equation, valid for all fluids:

$$\frac{\partial \rho}{\partial t} + \nabla \cdot (\rho u) = 0 \tag{3.8}$$

For an incompressible fluid ($\rho = constant$), this equation can be simplified into the following:

$$\nabla \cdot u = 0 \tag{3.9}$$

3.2.3 Conservation of linear momentum

Similarly to all continuous matter, fluids obey the momentum conservation law, which is more commonly known as Newton's Second law. This conservation can also be described as the notion that the sum of all forces applied to a system or, in this case, a control volume, is equal to the product of the mass and acceleration of the matter it contains.

This law is translated into the following equation, which balances gravity, static pressure and strain forces:

$$\rho g - \nabla p + \nabla \cdot \tau = \rho \frac{Du}{Dt} \tag{3.10}$$

where $\frac{Du}{Dt}$ is the material derivative of velocity:

$$\frac{Du}{Dt} = \frac{\partial u}{\partial t} + u_x \frac{\partial u}{\partial x} + u_y \frac{\partial u}{\partial y} + u_z \frac{\partial u}{\partial z} \tag{3.11}$$

When represented in each of its components, one obtains the momentum equations in their full form, which are valid for any fluid in any general motion.

$$\rho g_x - \frac{\partial p}{\partial x} + \frac{\partial \tau_{xx}}{\partial x} + \frac{\partial \tau_{yx}}{\partial y} + \frac{\partial \tau_{zx}}{\partial z} = \rho \left(\frac{\partial u_x}{\partial t} + u_x \frac{\partial u_x}{\partial x} + u_y \frac{\partial u_x}{\partial y} + u_z \frac{\partial u_x}{\partial z} \right) \tag{3.12}$$

$$\rho g_y - \frac{\partial p}{\partial y} + \frac{\partial \tau_{xy}}{\partial x} + \frac{\partial \tau_{yy}}{\partial y} + \frac{\partial \tau_{zy}}{\partial z} = \rho \left(\frac{\partial u_y}{\partial t} + u_x \frac{\partial u_y}{\partial x} + u_y \frac{\partial u_y}{\partial y} + u_z \frac{\partial u_y}{\partial z} \right) \tag{3.13}$$

$$\rho g_z - \frac{\partial p}{\partial z} + \frac{\partial \tau_{xz}}{\partial x} + \frac{\partial \tau_{yz}}{\partial y} + \frac{\partial \tau_{zz}}{\partial z} = \rho \left(\frac{\partial u_z}{\partial t} + u_x \frac{\partial u_z}{\partial x} + u_y \frac{\partial u_z}{\partial y} + u_z \frac{\partial u_z}{\partial z} \right) \tag{3.14}$$

3.2.4 Navier-Stokes Equations

A particular case of the momentum equations is when the fluid being analyzed has a Newtonian viscous behaviour and the flow can be considered isothermic. With these simplifications, one can obtain the stress tensor as a function of the deformation rate through equation 3.6, since the fluid's dynamic viscosity is constant.

$$\tau_{xx} = 2\eta \frac{\partial u_x}{\partial x} \tag{3.15}$$

$$\tau_{yy} = 2\eta \frac{\partial u_y}{\partial y} \tag{3.16}$$

$$\tau_{zz} = 2\eta \frac{\partial u_z}{\partial z} \tag{3.17}$$

$$\tau_{ij} = \tau_{ji} = \eta \left(\frac{\partial u_i}{\partial j} + \frac{\partial u_j}{\partial i} \right), \forall i \neq j \tag{3.18}$$

In result of this, we can substitute the stress tensor components in the momentum equations, obtaining the widely used Navier-Stokes equations [41]:

$$\rho g_x - \frac{\partial p}{\partial x} + \eta\left(\frac{\partial^2 u_x}{\partial x^2} + \frac{\partial^2 u_x}{\partial y^2} + \frac{\partial^2 u_x}{\partial z^2}\right) = \rho\left(\frac{\partial u_x}{\partial t} + u_x\frac{\partial u_x}{\partial x} + u_y\frac{\partial u_x}{\partial y} + u_z\frac{\partial u_x}{\partial z}\right) \quad (3.19)$$

$$\rho g_y - \frac{\partial p}{\partial y} + \eta\left(\frac{\partial^2 u_y}{\partial x^2} + \frac{\partial^2 u_y}{\partial y^2} + \frac{\partial^2 u_y}{\partial z^2}\right) = \rho\left(\frac{\partial u_y}{\partial t} + u_x\frac{\partial u_y}{\partial x} + u_y\frac{\partial u_y}{\partial y} + u_z\frac{\partial u_y}{\partial z}\right) \quad (3.20)$$

$$\rho g_z - \frac{\partial p}{\partial z} + \eta\left(\frac{\partial^2 u_z}{\partial x^2} + \frac{\partial^2 u_z}{\partial y^2} + \frac{\partial^2 u_z}{\partial z^2}\right) = \rho\left(\frac{\partial u_z}{\partial t} + u_x\frac{\partial u_z}{\partial x} + u_y\frac{\partial u_z}{\partial y} + u_z\frac{\partial u_z}{\partial z}\right) \quad (3.21)$$

3.2.5 Hagen-Poiseuille Flow

The Navier-Stokes equations are second order non-linear partial differential equations. In spite of this, some solutions for simple flows have been found. One of which, and the one of the most interest in the analysis of blood flow through the vessels, is the Hagen-Poiseuille flow, represented in figure 3.2 [41].

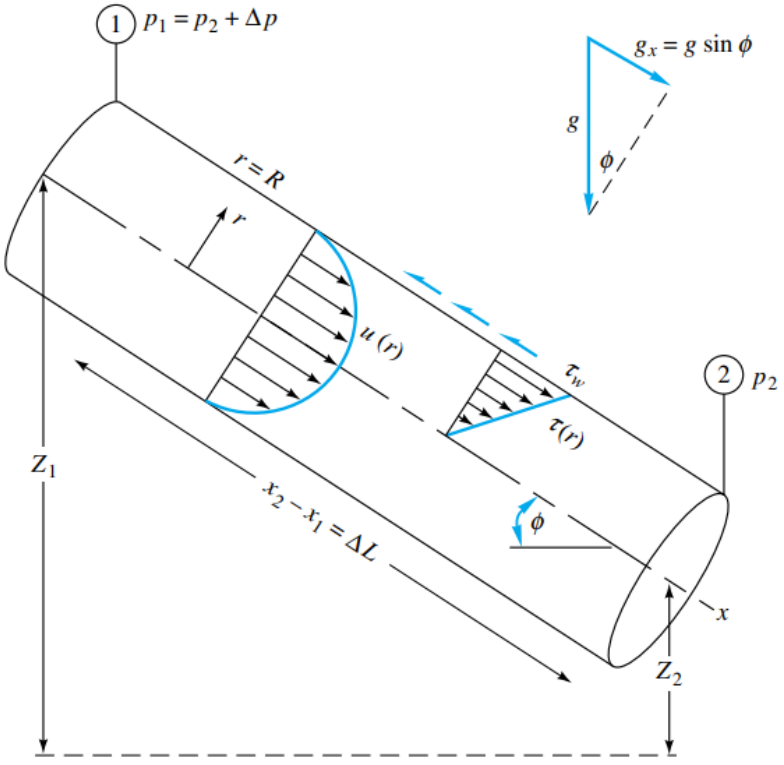

Figure 3.2: Hagen-Poiseuille Flow. Adapted from [41]

This is the designation given to a fully developed flow in a circular tube of constant cross section, driven by a constant pressure differential and/or gravity. Considering a cylindrical coordinate system, which simplifies the analysis of flow in circular pipes and is shown in figure 3.3 (the z axys represents the x axys present in figure 3.2), we can make the following assumptions [41] [27]:

- Steady flow: $\frac{\partial}{\partial t} = 0$

- No circumferential variation: $\frac{\partial u}{\partial \theta} = 0$;
- Fully developed flow: $\frac{\partial u}{\partial x} = 0$;
- A constant pressure gradient throughout the flow: $\frac{\partial p}{\partial x} = const.$

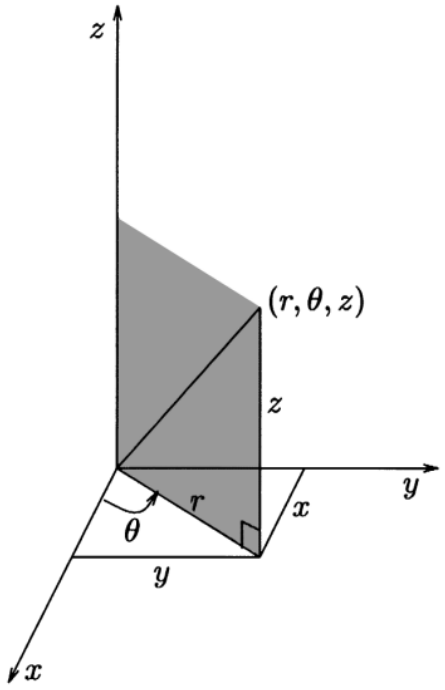

Figure 3.3: Cylindrical coordinate system. Adapted from [41]

The equations of interest in this problem are the continuity equation and the Navier-Stokes equation in the x axis, which represented in the cylindrical coordinate system have the following form [27]

$$\frac{1}{r}\frac{\partial}{\partial r}(ru_r) + \frac{1}{r}\frac{\partial}{\partial \theta}(u_\theta) + \frac{\partial u_x}{\partial x} = 0 \tag{3.22}$$

$$\rho g_z - \frac{\partial p}{\partial z} + \eta\left[\frac{1}{r}\frac{\partial}{\partial r}\left(r\frac{\partial u_z}{\partial r}\right) + \frac{1}{r^2}\frac{\partial^2 u_z}{\partial \theta^2} + \frac{\partial^2 u_z}{\partial z^2}\right] = \rho\left(\frac{\partial u_z}{\partial t} + u_r\frac{\partial u_z}{\partial r} + \frac{u_\theta}{r}\frac{\partial u_z}{\partial \theta} + u_z\frac{\partial u_z}{\partial z}\right) \tag{3.23}$$

The assumptions mentioned above let us simplify the continuity equation into the following form:

$$\frac{1}{r}\frac{\partial}{\partial r}(ru_r) = 0 \tag{3.24}$$

which can then lead us to the conclusion that $ru_r = constant$.

By the no slip boundary condition in the walls of the tube, which states that all velocity components are null, we can conclude that for $r = D/2$, v_r is equal to 0, making it necessary that $v_r = 0$ in all the flow's domain. Therefore, the fluid only flows in the x direction, what allows us to obtain the exact solution of equation 3.23 and thus obtain the velocity profile in a tube section perpendicular to the flow's direction [41]:

$$u_x(r) = \frac{1}{4\eta}\left[-\frac{\partial}{\partial x}(p-\rho gz)((D/2)^2 - r^2)\right] \tag{3.25}$$

where z is the vertical coordinate present in figure 3.2.

The profile obtained can be seen in figure 3.2, being parabolic with null values in the walls and a maximum in the center of the tube. Through integration of this equation across the section's area, we can then obtain an expression for the flow rate:

$$Q = \int_0^R u_x(r)dA = \frac{\pi(D/2)^4}{8\eta}\left[-\frac{d}{dx}(p+\rho gz)\right] \tag{3.26}$$

If we consider the tube horizontal, we obtain the result of Hagen's experiment, which gives the relationship between pressure drop and flow rate through a determined flow length, L [41]:

$$\Delta p = \frac{8\eta\Delta L}{\pi R^4}Q \tag{3.27}$$

One can then rearrange the equation to obtain the flow's resistance, R:

$$\frac{\Delta p}{Q} = \frac{8\eta\Delta L}{\pi(D/2)^4} = R \tag{3.28}$$

Although this results are derived from some simplifications that don't apply to blood circulation, such as the assumption of Newtonian fluid, the tube being rectilinear and horizontal and the flow steady and fully developed, it is still a good first representation of what happens physically in left coronary flow. Coronary flow is also propelled by a pressure differential, since the heart works as a pump and, if the deformation of the arteries walls is neglected, one can consider the blood vessels as rigid tubes. It is possible to understand that the vessel's resistance is of upmost importance when trying to draw conclusions about the evolution of pressure through the arteries, knowing the conditions of both flow-rate and pressure with which blood leaves the myocardium.

3.3 Governing equations for unsteady flow

Blood flow across the cardiovascular system can only be considered steady in small capillaries and veins. In large arteries, such as the LCA, it has pulsatory behaviour, which can be described

as the sum of a mean steady motion with a flutuation of the same order of magnitude [28].

3.3.1 Womersley Number

Although the Reynolds number gives great information about a fluid flow's properties, it doesn't account for the effects of transient phenomenon in unsteady situations. Since the heart pumps blood in a cycle, blood circulation is transient, with both the flow-rate and pressure varying through each cardiac cycle.

In order to retrieve information of the oscillatory effects in transient flow, one can use another adimensional parameter, called the Womersley number, Wo, which was developed by J. R. Womersley to be applied in blood flow [43]:

$$Wo = R\sqrt{\frac{\rho\omega}{\eta}} \tag{3.29}$$

R is the artery's cross section's radius and $\omega = \frac{2\pi}{T}$ is the angular frequency of the cardiac cycle, with T being its period.

Like the Reynolds number, the Womersley number represents the ratio between inertial and viscous forces, but instead accounts for the inertia due to oscillatory effects. The higher the Wo magnitude, the more unsteady effects will affect the flow, while values close to 0 make it closer to a purely steady scenario [28][29].

The Reynolds number can also be be utilized in transient flow despite this, considering the mean flow velocity or the amplitude of oscillation as reference.

3.3.2 Sinusoidal Oscillatory flow

We first consider a simple case of a flow similar to the Hagen-Poiseuille horizontal one, with the same coordinate system, but driven by a sinusoidal oscillatory pressure gradient, instead of a constant one:

$$\frac{\partial p}{\partial x} = \rho k sin(\omega t) \tag{3.30}$$

where k is a constant correspondent to the pressure gradient's amplitude.

Using the same assumptions as for the Hagen-Poiseuille flow, with the exception of steady flow, it is possible to develop equation 3.23, which is now time dependent, into the following [28]:

$$\rho\frac{\partial u_x}{\partial t} + \rho k sin(\omega t) = \eta\frac{1}{r}\frac{\partial}{\partial r}\left(r\frac{\partial u_x}{\partial r}\right) \tag{3.31}$$

With the same boundary conditions used to solve the Navier-Stokes equation of steady flow, we can obtain the velocity profile, expressed in terms of Wo [43] [28] [29]:

$$u_x(t,\ r) = \frac{k}{2\omega}\left[1 - \frac{J_0\left(\frac{r}{R}Wo\sqrt{\frac{-i\pi}{2}}\right)}{J_0\left(Wo\sqrt{\frac{-i\pi}{2}}\right)}\right] e^{i2\pi\frac{1}{T}} + c.c. \tag{3.32}$$

where J_0 is the Bessel function of the first type of order 0, with complex argument, and $c.c.$ is a complex factor included to ensure the final result is real [28].

The velocity profiles obtained through the oscillation for different Wo values are represented in figure 3.4 and allow one to better understand the influence that transient effects can have in pipe flow.

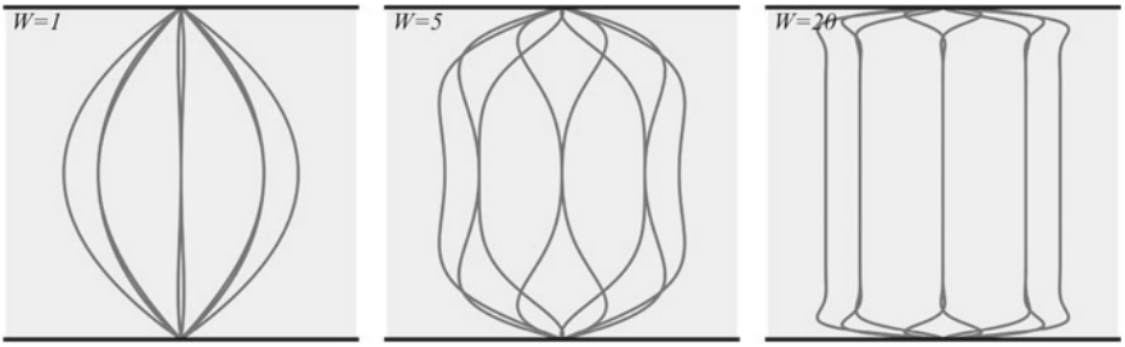

Figure 3.4: Oscillatory flow velocity profiles for various Womersley numbers. Adapted from [28]

Apart from the definition previously given, the Womersley number can also be presented as following:

$$Wo = \frac{D}{\sqrt{\nu T}} \tag{3.33}$$

where $\nu = \frac{\eta}{\rho}$ is the kinematic viscosity.

The thickness that the boundary layer of a flow reaches, which is the domain portion where viscous effects due to interaction with the wall are present, is considered proportional to $\sqrt{\nu t}$, with t being the time period passed. Since oscillatory flow happens in cycles with the duration of its period, T, the bottom part of equation 3.34 represents the maximum boundary layer thickness that an oscillating flow reaches. We can thus arrive at a new definition for the Womersley number, which is the ratio between the diameter of a flow's section and the correspondent boundary layer thickness.

For low Wo values, T has high magnitude and the flow has time to develop, what increases the thickness of the boundary layer and allows viscous effects to be distributed through most of the flow's domain. This makes the velocity profiles obtained very similar to which of the Hagen-Poiseuille case, since flow is close to fully developed.

When Wo has high magnitude, the opposite happens. Oscillations have small T values and, thus, the boundary layer lacks time to develop, which makes the viscous effects only affect flow near the wall and results in much higher velocity gradients in this area, deviating from the smooth parabolic profiles obtained for steady flow [28].

3.3.3 Pulsatile flow

As mentioned above, blood flow through the vessels is usually pulsatile: unsteady, periodic in time and with non-zero average velocity. Its pressure gradient is the sum of a mean constant with a series of sinusoidal oscillations, what makes the previous analysis of sinusoidal oscillatory flow of the upmost importance [28].

If we consider unidirectional flow in the same conditions and a pressure gradient represented by the following equation:

$$\frac{1}{\rho}\frac{\partial p}{\partial x} = -k + \sum_n U_n e^{i2\pi n \frac{t}{T}} \tag{3.34}$$

a solution can be obtained for the velocity profile through the combination of the Hagen-Poiseuille and sinusoidal oscillatory equations.

It is, thus, possible to conclude that the velocity profiles obtained will be the sum of a parabolic steady profile, like represented in figure 3.2, plus the particular solutions of sinusoidal flow, such as the ones represented in figure 3.4 [28].

A representation of the profiles obtained is present in figure 3.5, which contains velocity profiles correspondent to a constant mean flow rate and a single sinusoidal oscillation of amplitude equal to the mean flow, for different Womersley numbers. For low Wo values, the flow is, similarly to oscilatory sinusoidal flows, a series of parabolic Hagen-Poiseuille profiles. For high Wo values, the flow starts having recirculation, with inverted flow present in the boundary layer near the wall.

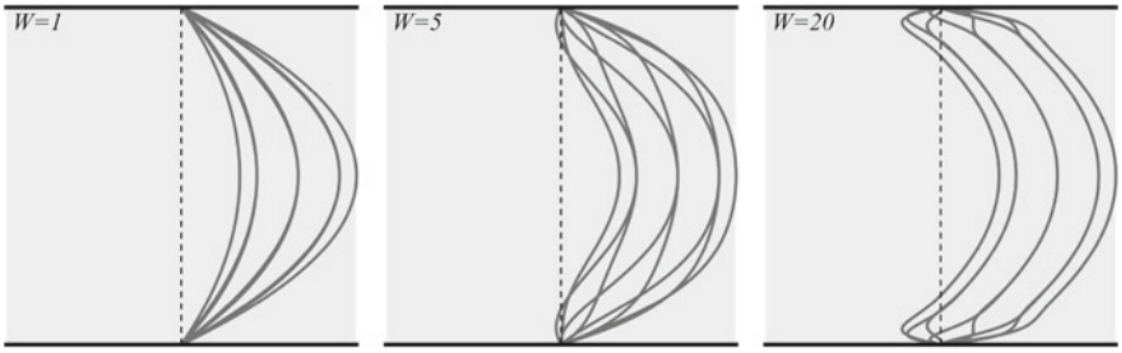

Figure 3.5: Pulsatory flow velocity profiles for various Womersley numbers. Adapted from [15]

Table 3.1 presents standard dimensions and values of both *Wo* and *Re* for different types of cardiovascular vessels [28]. These values help us identify which type of pulsatory flow, from the ones presented in figure 3.5, might be the most representative of the circulation in each vessel.

Table 3.1: *Wo* and *Re* values for different types of vessels

	$U(cm/s)$	$D(cm)$	*Re*	*Wo*
Aorta	100	3	10000	20
Middle arteries	30	1	1000	5
Small arteries	5	0.2	30	1
Arterioles	0.1	< 0.1	< 0.5	< 0.5

The LCA is considered a middle artery, which makes it possible to conclude that the transient effects will be of importance in the analysis of blood flow through the various vessels, thus needing special attention in the modeling procedure.

Chapter 4

Hemorheology

As discussed in the previous chapter, the relationship between shear stress and flow rate is one of the key elements when studying fluids' flow. This makes rheology, which is the study of the deformation and flow of matter, a very important component of blood flow analysis [22].

Blood is a complex non-Newtonian fluid that has both viscous and elastic behaviour. This creates a need for understanding of blood's composition and its rheological behaviour, this field of study is known as of hemorheology [17].

4.1 Blood's composition

Blood is a 2-phase fluid, comprised of cells suspended in a liquid extracellular matrix, blood plasma. It is generally considered a fluid with the exception of abnormal cases where it can develop semi-solid behaviour due to the process of clothing. The combination of both blood and its blood cell producing tissue accounts for more than 10% of a person's mass[17][4].

4.1.1 Plasma

Plasma is a solution composed of low-molecular-weight-solutes, proteins and water. Its principal components are the following [4] [17][16]:

- Water: representing around 90% of blood's mass;
- Low molecular weight components: Na^+, K^+, Ca^{2+}, HCO_3^-, and $C_6H_{12}O_6$ (glucose) are the most important, with its concentrations being regulated by the kidneys and the lungs;
- Proteins: thousands of proteins and peptides are contained in plasma, which include trace levels of hormones and substantial concentrations of immunoglobulins. The liver synthesizes numerous plasma proteins, of which the most abundant are albumin, fibrinogen and α and β globulins.

Under regular conditions, plasma plays a minimal role in determining blood's viscosity, however, under pathological conditions in which plasma proteins increase, specially fibrinogen, plasma viscosity increases with negative effects for blood flow, specially in microcirculation [17].

4.1.2 Cells or formed elements

The cells present in blood can be divided into three classes [4] [17]:

- Red blood cells (RBCs), or erythrocytes: the only cells that normally remain in blood during their entire lifespan. They are membrane-bound containers of hemoglobin, specialized in carrying O_2 and CO_2 between lungs and tissues. RBCs account for $40-50\%$ of total blood volume and 99% of total blood cells;
- White blood cells (WBCs), or leukocytes: these cells travel for variable time lengths in blood until they eventually exit the vessels into another tissue or undergo apoptosis. They consist of granulocytes, monocytes and lymphocites and are part of the immune system, as residents of connective tissue, protecting the body against infection;
- Platelets, or thrombocytes: cell fragments which prevent blood loss from vessels. While regularly inactive, when a vessel is ruptured, platelets come in contact with collagen what, combined with other factors, makes them interact with the fibrin clot that forms the lesion and help close ruptures. Furthermore, platelets also release factors from their granules that stimulate fibroblasts and other cells to migrate to the lesion's area and help repair it. In terms of overall volume, they have a even smaller value than WBCs.

In terms of blood viscosity, RBCs are the most influential cells in both large vessel flow and microcirculation. WBCs have negligible effects in blood circulation in larger vessels, however, they play a major role in blood's microcirculation, due to its internal content having greater viscosity and density than that of the erythrocytes and their larger size and increased stiffness. Platelets are negligible in terms of blood flow behaviour in all vessels due to their much smaller size than both RBCs and WBCs [17].

4.2 Fluid categories

In terms of its viscosity, a fluid can be divided into different categories. An inviscid fluid as a negligible viscosity, which makes its value be approximated by 0, while fluids of nonzero viscosity are called viscous. The latter fluids can be further divided into the following types [22] [23] [41] [27]:

- Fluids in which the shearing stress is directly proportional to the rate of shearing strain are called Newtonian Fluids. This makes the fluids' viscosity a constant for all magnitudes of shear strain ($\eta = const.$).

- Cases in which this relationship isn't proportional are called non-Newtonian, for which the most common cases are represented in figure 4.1, where the viscosity is dependent on the second invariant of the rate-of-strain tensor: $II_D = \frac{1}{2}((tr(D))^2 - tr(D^2))$, $tr()$ being the trace operator, that retrieves the summation of a matrix's principal diagonal's components. These fluids can be further divided into Generalized Newtonian fluids (GNFs), which still abide to equation 3.6 but have varying values of viscosity that depend on the strain rate, and viscoelastic fluids, which have both viscous and elastic properties. If a fluid's viscosity increases with an increase of shear rate, it is categorized as shear thickening, while the opposite is called shear-thinning.

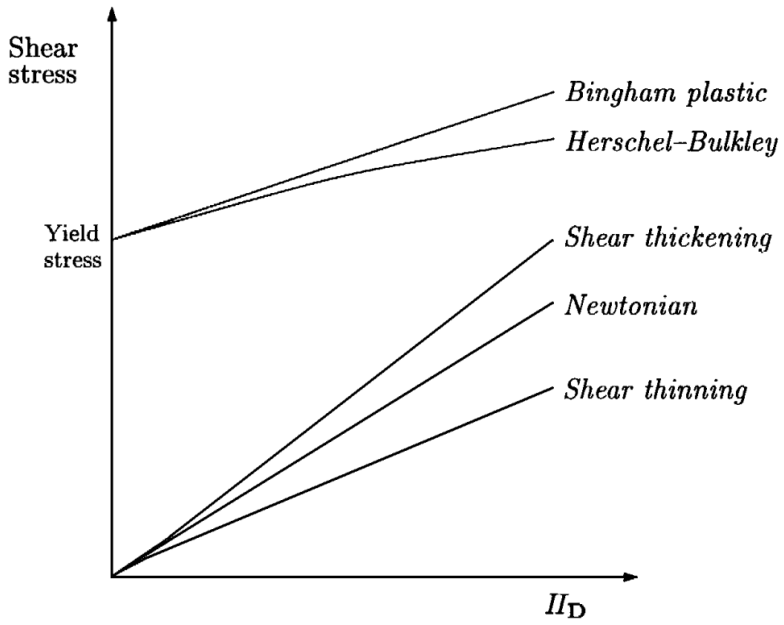

Figure 4.1: Behaviour of non-Newtonian fluids. Adapted from [27]

4.3 Generalized Newtonian models

Non-Newtonian fluids' rheological behaviour is harder to express, which leads to more complex models than equation 3.6. With this objective, models are developed for each specific fluid, in order to adjust viscosity functions that are representative of their behaviour.

As discussed above, GNFs don't have elastic behaviour. They abide by the Newtonian fluid's law, with the alteration that its viscosity is dependent on the shear rate, resulting in the generalized Newtonian fluid constitutive equation [22]:

$$\tau = \eta(\dot{\gamma})\dot{\gamma} \tag{4.1}$$

where $\dot{\gamma} = 2D$ is the shear rate.

From this equation, several models have been developed for η in order to be adjusted to different fluids. Some of the most prominent are described in the following [22]:

- Power-law model: defines viscosity with a function proportional to some power of the shear rate:

$$\eta(\dot{\gamma}) = m\dot{\gamma}^{n-1} \tag{4.2}$$

  where m is related to the magnitude of the viscosity and n its evolution with shear rate variation. For values of $n > 1$, the fluid is shear thickening, while for values of $n < 1$, the fluid is shear-thinning. When $n = 1$, the fluid has constant viscosity and, thus, is Newtonian.

  This model leads to simple calculations due to the existence of only two parameters, m and n, and has proven to be successful in predicting flow rate vs pressure drop measurements.

- Carreau-Yasuda model: this model captures more details of viscosity vs shear rate relationship and is represented by the following function with five parameters:

$$\frac{\eta(\dot{\gamma}) - \eta_\infty}{\eta_0 - \eta_\infty} = [1 + (\dot{\gamma}\lambda)^a]^{\frac{n-1}{a}} \tag{4.3}$$

  where η_∞ is the viscosity value for large $\dot{\gamma}$ values; η_0 is similar but for small $\dot{\gamma}$ magnitudes; a is the exponent and λ the time constant of the fluid, which influences are described in figure 4.2; n is similar to the exponent of the power-law model.

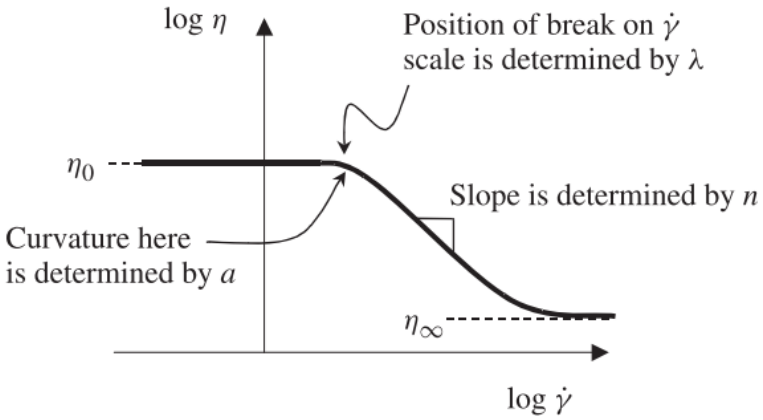

Figure 4.2: Viscosity curve predicted by the Carreau-Yasuda model. Adapted from [22]

Both the power-law and the Carreau-Yasuda models have proven success in predicting pressure vs flow rate measurements, which are the most important in the analysis of blood flow through the vessels. The latter brings more detail to the viscosity values for intermediate flow rates, while

having the downside of needing the determination of three more parameters when compared to the power-law. It has been extensively utilized in blood flow analysis, describing blood's shear-thinning behaviour. Nevertheless, it still fails to account for deformation in the fluid due to normal stresses, a consequence of the negligence of elastic behaviour [32][32].

It is, thus, productive to analyze more complex models which take into account blood's viscoelastic properties.

4.4 Viscoelastic model for blood

Although plasma is essentially a Newtonian fluid, the cells that it transports, specially RBCs, give it non-Newtonian properties. Furthermore, the deformation of these cells also makes blood have viscoelastic properties, which need to be taken into account [32] [17].

The most common viscosity models used in hemorheology are that of GNFs. In spite of this, the importance of taking into account blood's viscoelasticity properties is well documented in the literature. The viscoelastic properties can be neglected when a flow is close to steady state, which is not the case of blood flow, where the transient pumping of the heart and the curves and roughness of the vessels make the flow change rapidly with time. This is further accentuated in small vessels and in cases where stenosis are present, further disrupting the flow and making viscoelastic effects more relevant [32] [22].

This work follows the study realized by Pinto, *et al.* (2020), which compared a Newtonian model, a Carreau-Yasuda model and three different viscoelastic constitutive models, in order to analyze the differences in results when applied to blood circulation calculus in the right coronary artery (RCA). The conclusion was that the viscoelastic models were a major improvements of both the Newtonian and the Carreau-Yasuda, which was expected due to the coronary arteries being of lower diameter, accentuating viscoelastic effects. Furthermore, the multi-mode simplified Phan-Thien/Tanner model (sPTT) was the most accurate of all, thus being the one chosen by the author for LCA blood flow simulation, since its thickness is of similar magnitude as the RCA [32].

4.4.1 Simplified Phan-Thien/Tanner model

To serve as a starting point of reference, the general linear momentum conservation equation is again presented:

$$\rho g - \nabla p + \nabla \cdot \tau = \rho \frac{Du}{Dt} \tag{4.4}$$

The sPTT model gives us constitutive equations for the stress tensor's, τ, Cartesian components [36][32]:

$$\tau_{ij} = \tau_{ij_s} + \tau_{ij_e} \tag{4.5}$$

$$\tau_{ij_s} = -2\eta_s D_{ij} \tag{4.6}$$

$$\tau_{ij_e} = \sum_{k=1}^{N} \tau_{ij_k} \tag{4.7}$$

in which equation 4.5 splits the stress tensor into solvent and elastic contributions. The solvent one is described by equation 4.6, being caused by viscous stresses. The elastic contribution is described by the multi mode formulation present in equation 4.7, which, in the case of an sPTT model, satisfy the following equation:

$$\left(1 + \frac{\lambda_k \varepsilon_k}{\eta_{e_k}} tr(\tau_{ij_k})\right) \tau_{ij_k} + \lambda_k \widehat{\tau}_{ij_k} = -2\eta_{e_k} D_{ij_k} \tag{4.8}$$

where $\widehat{\tau_{ij_k}}$ are the Cartesian components of the elastic stress tensor's upper convected derivative [22]:

$$\widehat{\tau_k} = \frac{D\tau_k}{Dt} - (\nabla \cdot u)^T \cdot \tau_k - \tau_k \cdot \nabla \cdot u \tag{4.9}$$

The model has four modes $(N = 4)$, with three coefficients each: λ_k, the relaxation time; η_{e_k}, the elastic viscosity; ε_k, the extensibility coefficient [32] [8].

For further details about the sPTT model utilized, the reader is referred to [8], where the model's development is described.

Chapter 5

Lumped-parameter models for coronary outflow

When simulating blood flow, it is virtually impossible to directly represent the heart and the over 5 billion blood vessels of the cardiovascular system. Therefore, the simulation of blood flow requires a 3D model of the most relevant portion of the circulatory system and boundary conditions for all of the chosen domain's limits. More specifically, it is necessary that one prescribes conditions for either flow or pressure in the vessels' inlets, outlets and walls. From these, the most complex is the choice of outflow boundary conditions for the outlets, which have a significant influence in the flow rate and pressure through the 3D model [5].

The most common choice for outflow boundary conditions are prescribed velocity or pressure values. In this work, this is not practical for a number of reasons, of which the most important is that the blood flow exiting the branches of the model and the pressure distributions through it are the intended results of the simulation, which makes previous measurements of pressure or blood flow in the outlets not compatible with a non invasive calculation of FFR.

Various boundary conditions have been utilized in coronary outflow that don't require the specification of either flow rate or pressure. A common one is the resistance boundary condition, which has negative impact on transient flow modulation, requiring flow rate and pressure waves to be on phase. Another one consists of using 1D models for the downstream vessels, which need to be linearised due to the inability to solve non-linear transient equations for the millions of vessels downstream of the coronary artery. These options lack when modeling the non periodic effects in blood circulation, such as transitional or turbulent flow [38].

In this work, lumped (0D) parameters models will be utilized as boundary conditions for the models' outlets. This way of modelling blood flow will be explored in the present chapter.

5.1 Lumped-parameter models

The relationship between pressure and flow rate in a vascular tree structure of tube segments, such as the circulatory system, is a very complex problem. It depends on the individual characteristics of each tube (diameter, length and elasticity), the form of the driving pressure and alterations to flow in the their junctions.

A way of dealing with this problem is the utilization of lumped-parameter models, which reduce the vascular structure to a single tube, having representative properties of the whole network. By neglecting the spacial variations of the parameters and variables of flow, we can reach a set of ordinary differential equations that represent the relationship between pressure and flow similarly to the one observed in the physiological system but without the Herculean task of determining it through all the coronary vascular branches.

In the particular case of coronary flow, the objective is to find a correlation between pressure and flow in the inlet of the 3D model and pressure in its outlets, by modulating both the systemic and capillary circulation downstream of the section. The three most important parameters of these kind of models are resistance, inductance and capacitance, which modulate the principal characteristics of blood flow [44][38].

5.1.1 Resistance

Flow can be resisted by a number of factors. Both fluid inertia and wall elasticity can provoke resistance to the flow, but can also have the effect of aiding it. In a transient periodic flow, they oscillate between these two effects.

The most important factor of resistance to flow is thus its viscosity, with the viscous tensions always contributing to the resistance to flow. In this work, we will consider resistance, R, only as the viscous effects that dissipate energy in flow. Like it was mentioned in chapter 3, viscous stresses are present in the boundary layer of a flow, through a combination of the no-slip boundary condition at the wall and the viscous properties of the fluid.

The total viscous resistance to flow can be represented by the following equation, as referenced in chapter 3 [16] [44]:

$$R = \frac{\Delta p}{Q} \Leftrightarrow Q = \frac{\Delta p}{R} \tag{5.1}$$

and is thus defined as the amount of pressure differential required to produce a given amount of flow.

Let us now recapture equation 3.28:

$$R = \frac{8\eta\Delta L}{\pi R^4} \tag{5.2}$$

which is only applicable to the Hagen-Poiseuille flow. Though it is a simplified flow, not applicable to blood circulation, we can notice that R is highly dependent on the vessel's radius, due to it being inversely proportional to its fourth power.

The mathematical relationship between a vessel's radius and flow rate in blood circulation was first proposed by Murray, stating that it was proportional to the vessel's diameter, D, to a k power [24]:

$$Q \propto D^k \tag{5.3}$$

Since R is inversely proportional to Q, which can be concluded through equation 5.1, we can then adapt Murray's law to the resistance to flow:

$$R \propto D^{-k} \tag{5.4}$$

k is an empirical parameter, which was first proposed to have the value of 3.

Murray's law, in its simplest form, is the manifestation of adaptive mechanisms by which blood vessels remodel in function of the shear stress magnitude in the surface. In larger vessels, this value of k is not applicable, with the value of 2.1 being recommended for the LAD and LCx. This deviation is explained by the fact that Murray's formulation took coronary circulation tree as an integrated system rather than looking at each vessel segment individually [21] [24].

Through equation 5.4, we can see that the smaller the vessel's diameter, the more resistance to the flow will be present. This effect is slightly attenuated in the LAD and LCx, which will have a bigger resistance due to the smaller value of k. Due to this, about two thirds of the resistance to blood flow in the whole systemic circulation is present in the small arterioles.

In order to obtain the resistance to flow in the whole blood circulation, one must combine the resistances of different vessels to obtain general values. This can be done by combining vessels arranged in series or in parallel, such as shown in figure 5.1.

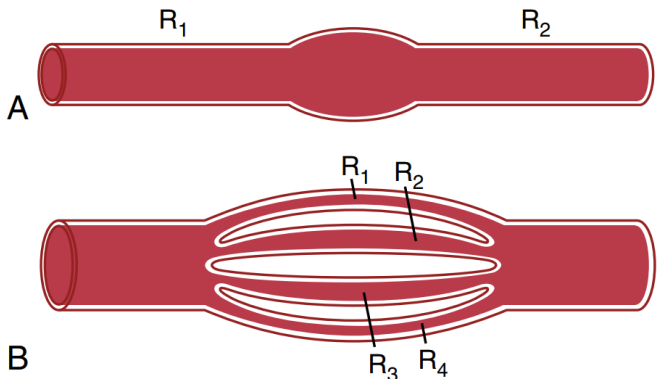

Figure 5.1: Vascular resistance. **A**, in series. **B**, in parallel. Adapted from [16]

In the case of vessels in series, we can combine their resistances by summing each individual values:

$$R_{tot} = R_1 + R_2 \tag{5.5}$$

For parallel vessels, the following equation can be applyed:

$$\frac{1}{R_{tot}} = \frac{1}{R_1} + \frac{1}{R_2} + \frac{1}{R_3} + \frac{1}{R_4} \tag{5.6}$$

We can conclude that for arrangements in series, the addiction of an additional vessels will increase the resistance. On the contrary, in parallel vessels, the addition of a vessel will decrease the total resistance, which may seem a bit counter intuitive, but happens due to it being an extra pathway for blood to flow. Capillaries are smaller than the arterioles, but the latter have the largest contribution to the resistance, as previously stated, due to the much larger number of capillaries arranged in parallel, which makes the overall resistance smaller.

It is thus possible for us to combine the resistance of each vessel tree by both equations 5.5 and 5.6, and then sum them in order to obtain the whole resistance of the systemic circulation [16] [44]:

$$R_{sys} = R_{arteries} + R_{arterioles} + R_{capillaries} + R_{venules} + R_{veins} \tag{5.7}$$

5.1.2 Inductance

Acceleration in a fluid can occur in both space and time. In steady state flows, only spacial acceleration occurs, which may be caused by a narrowing of flow path or at the entrance of a vessel. In unsteady flows, a change in the driving pressure provokes the variation of the velocity in each point with time, instead of just changing in space.

The fluid doesn't respond immediately to an acceleration, due to its inertia. When the driving pressure changes to a higher magnitude, the flow rate takes some time to adjust and increase its value. This lag between pressure and subsequent flow rate changes is a form of resistance to flow and is called inductance, L.

As R relates the pressure differential necessary to a certain flow rate, L relates the pressure differential, Δp_L, that a certain change in flow rate through time, $\frac{dQ}{dt}$, provokes, through the following equation:

$$\Delta p_L = L\frac{dQ}{dt} \tag{5.8}$$

This relation can be derived from Newton's second law which, applied to a mass, m, can be defined by the following equation, with x being its position and F the driving force:

$$m\frac{d^2x}{dt^2} = F \tag{5.9}$$

If we apply equation 5.9 to a mass of fluid flowing in a tube, we can obtain newton's equation for pipe flow. By assuming that viscous effects are not present, we can consider a cylindrical volume of fluid that moves freely through the tube, as a bolus. Furthermore, the driving force in the case of pipe flow is a pressure differential applied to the circular faces of the cylinder and we can apply Newton's second law by the following equation:

$$\rho V\frac{du}{dt} = \Delta p_l A \Leftrightarrow \rho\frac{\pi d^2}{4}l\frac{du}{dt} = \Delta p_L\frac{\pi d^2}{4} \Leftrightarrow \Delta p_l = \rho l\frac{du}{dt} \tag{5.10}$$

where ρ is the fluid's density, V is the volume of fluid considered, A is the area of the tube's section, d is its diameter and u is the velocity.

Since velocity is taken as constant through the whole section, the flow rate can be calculated simply by the product of velocity and section area:

$$Q = uA = u\frac{\pi d^2}{4} \tag{5.11}$$

We can then combine both equations 5.10 and 5.11 to obtain the following:

$$\Delta p_l = \frac{4\rho l}{\pi d^2}\frac{dq}{dt} \tag{5.12}$$

When comparing this equation to 5.8, we can arrive at the value for L:

$$L = \frac{4\rho l}{\pi d^2} \tag{5.13}$$

We can see that, as happens with R, arteries with lesser diameters will have a bigger inductance, resulting in more resistance to flow. The higher the inductance, the more resistance to flow there will be when the flow is accelerated or decelerated.

By combining both resistance with inductance effects, we can arrive at a total pressure difference, Δp, that is required to overcome both resistances due to inductance, Δp_L, and viscous effects, as in discussed previously in section 5.1.1, Δp_R [44]:

$$\Delta p = \Delta p_R + \Delta p_L = RQ + L\frac{dQ}{dt} \tag{5.14}$$

5.1.3 Capacitance

A valuable asset of all blood vessels is their distensibility. This property allows them to accommodate the variations of blood output from the heart and average out the resulting pressure pulsations. The property that analyzes this capability is capacitance, C, which represents the total quantity of blood that can be stored in a given segment of the circulation for a singular increase in the pressure differential propelling blood flow [16]:

$$C = \frac{\Delta V}{\Delta(\Delta p)} \tag{5.15}$$

We can arrive at another definition for compliance, which is the amount of change in the pressure differential, Δp, needed to produce a certain change in the volume of a vessel segment, V.

It is important to note that the compliance of a vessel depends not only on its distensibility but also on its size, since compliance is the distensibility of a vessel multiplied by its volume.

Capacitance affects the total volume of the vessel, therefore flow rate may vary from its entrance to its exit because some flow may be utilized to inflate the vessel and some blood at the exit may have come from its deflation.

In blood flow, working with the concept of volume isn't a useful parameter to work with. Instead, it is much more practical to use the flow rate of blood through the vessels, Q. Since blood is considered an incompressible fluid for the ciruclatory system, a change in volume can only be achieved by a certain amount of flow rate that fills the arteries and increases their volume, the capacitive flow rate, Q_c. Considering this flow rate constant, we can get the change in volume that occurs after a period of time, Δt:

$$\Delta V = Q_c \Delta t \tag{5.16}$$

We can combine equations 5.15 and 5.16 to obtain the following expression for C:

$$C = \frac{Q_c \Delta t}{\Delta(\Delta p)} \tag{5.17}$$

therefore:

$$Q_c = C\frac{\Delta(\Delta p)}{\Delta t} \tag{5.18}$$

Considering Δp as continuous in time, we can obtain Q_c as a function of time as well:

$$Q_c = C\frac{d(\Delta p)}{dt} \tag{5.19}$$

We can thus conclude that C describes the proportional relationship between flow rate used to either inflate the vessel or deflate it and the variation in the pressure differential, with bigger C values corresponding to bigger magnitudes for Q_c. Positive pressure differential variations cause an inflation of the vessels and thus Q_c is positive, while negative values cause the exact opposite.

In order to obtain the full flow rate in the vessel, we can sum the circulatory flow rate (resistive), Q_r, with the capacitive flow rate, Q_c:

$$Q = Q_r + Q_c \tag{5.20}$$

In blood flow, pressure varies through time in a cyclic manner. A specific case that is useful to illustrate how flow rate will develop with the changing of Δp is by considering an oscillatory pressure evolution:

$$\Delta p = \Delta p_0 sin\omega t \tag{5.21}$$

where Δp_0 is a constant and ω is the angular frequency of the oscillation.

Utilizing this function in equations 5.1 and 5.19, we obtain functions for both Q_r and Q_c:

$$Q_r = \frac{\Delta p_0}{R} sin\omega t \tag{5.22}$$
$$Q_c = \Delta p_0 \omega C cos\omega t \tag{5.23}$$

We can thus see that an oscillatory flow produces a resistive flow rate that is independent of the capacitance and which wave form is in sync with the pressure gradient. On the other hand, it also produces a capacitive flow which is scaled by the factor ωC, and thus increases in magnitude with higher capacitance values and has similar ω and a phase of 90° in comparison to Δp.

These results bring clarity to the importance of capacitance in oscillatory flow for distensible systems, which makes very important to the dynamics of coronary circulation. A very important component that is now revealed is studying the amount of the oscillatory flow that goes into inflating and deflating the vessels. The pressure differential driving coronary flow is a mix of both constant and harmonic parts, like referenced in chapter 3. Since the constant and oscillatory components of flow are not separated, the capacitance of the system affects both resistive flow as well as capacitive flow [44] [16].

5.1.4 Electrical Analogy

Using the parameters presented, the dynamics of coronary blood flow can be modelled as an electric circuit. This is only possible through the utilization of the lumped model described previously that represents the circulation tree using a single tube that is representative of the collective properties. The electrical analogy has been utilized extensively in modelling coronary flow, due to electrical circuits being very easy to manipulate and able to be tested experimentally.

Each relevant parameter of blood flow will have an electrical parameter that represents it. Electric potential or voltage, V, corresponds to the pressure difference, Δp, and electric current, I, corresponds to the flow rate, Q. The analogy is based on the fact that the relationship between potential across and current into different electrical components. By utilizing the concepts of resistance, impedance and capacitance built in the previous section, we can arrive at these relationships:

- The relationship between current and voltage across a resistor, R, is analogous to the relationship between pressure difference and flow rate in a vessel:

$$\Delta p = RQ \tag{5.24}$$
$$V = RI \tag{5.25}$$

- Voltage and current variation in an inductor, L, have a similar relation as a vessel's pressure difference and flow rate variation:

$$\Delta p = L\frac{dQ}{dt} \tag{5.26}$$
$$V = L\frac{dI}{dt} \tag{5.27}$$

- The same happens between voltage variation and current in a capacitor and pressure difference variation and flow rate in a vessel:

$$Q = C\frac{d(\Delta p)}{dt} \quad \Leftrightarrow \quad \Delta p = \frac{1}{C}\int Q dt \tag{5.28}$$
$$V = \frac{1}{C}\int I dt \tag{5.29}$$

As seen previously, the viscous resistance, R, gives the proportional relationship between flow rate and pressure difference, however, this is only applicable to steady flow. For oscillatory flow, there is an added form of resistance due to the presence of inductance and capacitance, which is called "reactance", S.

Combining both the resistance and reactance present in a transient flow, such as blood circulation, we arrive at a global parameter that correlates pressure difference, Δp, and flow rate, Q, representing the total impediment to flow, which is called impedance, Z.

This is a parameter belonging to the complex domain, with R being its real component and S its imaginary one:

$$Z = \frac{\Delta p}{Q} = R + iS \tag{5.30}$$

where i is the unit imaginary number.

This notation offers concise information on the influence of impedance on both the modulus and phase of complex pressure waves, characteristic of transient flow, while maintaining the simple relationship between pressure and flow rate. Furthermore, the rules for parallel and serial resistances can also be applied to impedances, making it possible to arrive at a global value for each model.

All three elements of the electrical model discussed before (R, L and C), can be converted into a corresponding impedance, which enables us to obtain governing equations in the complex domain [44]:

$$Resistance : Z = R \tag{5.31}$$

$$Inductance : Z = i\omega L \tag{5.32}$$

$$Capacitance : C = \frac{1}{i\omega C} \tag{5.33}$$

5.2 Windkessel models

Windkessel models are based on the hemodynamic description of the arterial circulation in terms of its resistance, inductance and capacitance. It was first described by Otto Frank, linking it to the German designation of an air chamber used in fire engines [34]. This engines turn the sinusoidal pump pressure generated into constant water stream, likewise, the circulatory system turns the heart's transient pressure into constant blood flow through the vessels. This behaviour corresponds to the Windkessel effect, and is illustrated in figure 5.2 [6].

As figure 5.2 suggests, the elasticity of the arteries as the same function as the air reservoir, the "Windkessel", in the water pump. By being able to inflate and deflate, the compliance effect discussed in the previous section, the arteries accumulate blood when inflating and propel it through the circulation when deflating, achieving a rather constant peripheral blood flow.

5.2.1 Two-element Windkessel model

The most basic Windkessel model makes use of the electrical analogy and consists of a resistance and a compliance element in parallel.

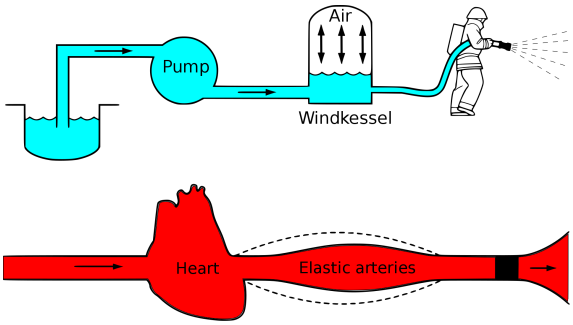

Figure 5.2: Windkessel effect. Adapted from [6]

Being the simplest of the Windkessel models, it takes into account the effect of arterial compliance and total peripheral resistance. Like mentioned in section 5.1.1, most of the arterial viscous resistance will be present in the smaller arteries and arterioles, thus, the resistance element of the model is the sum of all microcirculation tree vessel's resistances. On the contrary, the compliant element is largely obtained by the elasticity of the larger arteries, though being calculated by the sum of all vessel's compliance.

In circulation, blood has the option of moving either against the resistance or compliance, that is, moving forward in circulation or towards inflating the vessels. This is why the resistance and capacitance are located in parallel in the circuit. If coronary flow was steady, the most simple model could have just a resistance, relating pressure difference to flow rate, but, as it is a transient phenomenon, it is necessary to also take into account the effect of capacitance [44] [40] [9].

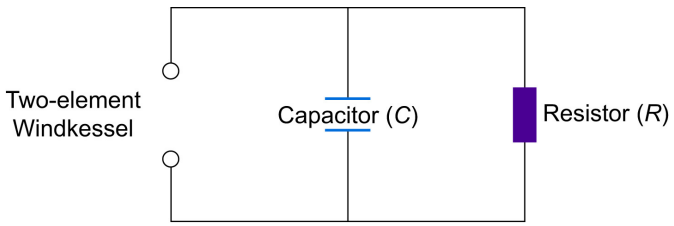

Figure 5.3: Two-element Windkessel model. Adapted from [35]

Through this model and utilizing the flow rate equations 5.24 and 5.28, we can obtain the following differential governing equation [9]:

$$Q(t) = \frac{P(t)}{R} + C\frac{d(P(t))}{dt} \tag{5.34}$$

Furthermore, utilizing the rule for parallel impedances, we can obtain the global complex impedance for the model, $Z(\omega)$ [44]:

$$\frac{1}{Z} = \frac{1}{R} + i\omega C \quad \Leftrightarrow \quad Z = \frac{R}{1 + iR\omega C} \tag{5.35}$$

The pressure waveform can be decomposed into a constant mean value and a series of harmonic oscillations, such as described in chapter 3. This is also applicable to the impedance, which will be different for each harmonic:

$$Z_n = \frac{R}{1 + iR\omega_n C} \tag{5.36}$$

with $\omega_n = 2\pi n$ and $n = 1, 2, 3, ..., N$, n being the particular harmonic and N the number of harmonics of the pressure waveform.

This two element model can predict the decay of aortic pressure during diastole, which is exponential, but fails to predict the relationship between pressure and flow during the systole. Through the measurement of input impedances in mammals, it was concluded that for higher frequencies its modulus tended to a plateau and its phase to 0°, while with this model, we obtain a modulus tending to 0 and a phase to 90°. This made researchers experiment with the addiction of more elements to the Windkessel model in order to improve it [40] [44].

5.2.2 Three-element Windkessel model

In the three-element model, we couple the parallel resistor and capacitor with a characteristic impedance of the aorta in series. This additional parameter links the lumped-parameter models with the wave travel aspects of the arterial circulation. The two-element model implies that driving pressure and resistance would be constant over the whole network, which doesn't happen due to the fact that it comprises an elastic component that makes vascular resistance and flow vary over time with pressure.

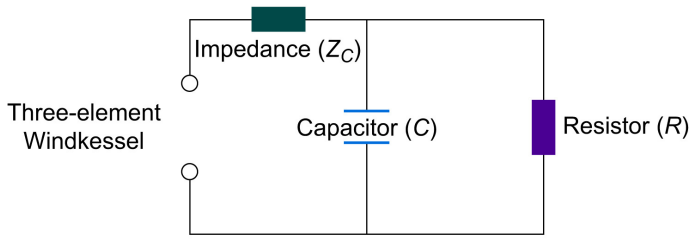

Figure 5.4: Three-element Windkessel model. Adapted from [16]

This model represents a major improvement on the 2-element one for higher frequencies, since the latter failed to predict flow behaviour during systole in this area. This makes it a common outflow boundary condition for coronary hemodynamics, such as represented in figure 5.5 [40] [35] [9].

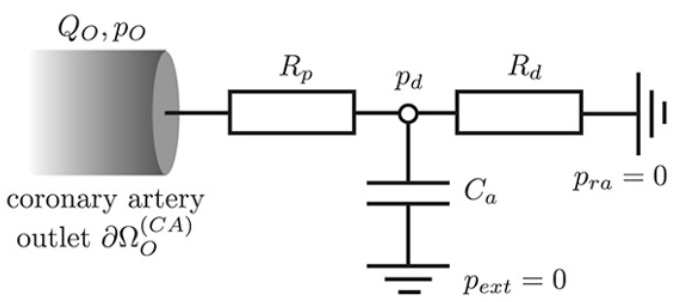

Figure 5.5: Three-element outflow boundary condition. Adapted from [16]

In this figure, Q_0 and p_0 are the flow rate and pressure in the outlet of the artery, R_p and R_d are, respectively, the proximal and distal resistances. C_a is the total compliance of downstream arteries and p_d is the distal pressure which corresponds to the pressure in the arterioles and capillaries [19]. It is of notice that the aortic impedance is represented as a resistance due to the fact that it has the same dimension as a resistor and, although it causes errors on the low frequencies range of input impedance, this parameter accounts for about 5 to 7% of the peripheral resistance and thus these errors can be neglected [40].

Through this model, we can arrive at the following governing equations for blood flow, utilizing the same principles as for the 2-element model [9] [19]:

$$\frac{dp_d}{dt} + \frac{p_d}{C_a R_d} = \frac{Q_0}{Ca} \tag{5.37}$$

$$p_0 = p_d + R_p Q_0 \tag{5.38}$$

The overall predicted wave forms through this model are close to measured ones and the global aspects of input impedance and pressure are well described by it. However, it generally overestimates arterial compliance, underestimates aortic characteristic impedance and produces significant errors at low frequency levels. Furthermore, the measured impedance has two maximums and a discrete minimum, while the one obtained with this model shows neither of these, as can be seen in figure 5.6:

We can see that for high frequencies, the three-element model produces very good results, however, it still has errors for the lower frequencies, which makes it possible to add elements to the model in order to improve it [40] [35] [37].

5.2.3 Five-element Windkessel model

By looking at figure 5.6, we can see that a four-element Windkessel model improves on the three-element one, but still doesn't translate the practical measurement's secondary maximum and discrete minimum of impedance in the various harmonics. In order to account for this and better

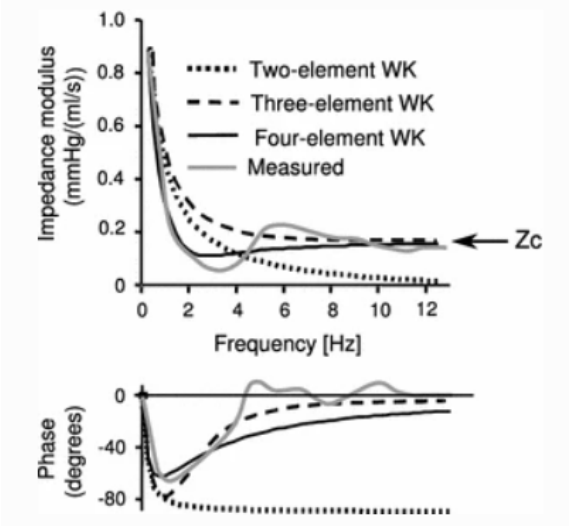

Figure 5.6: Impedance curves with different Windkessel models. Adapted from [40]

approximate reality, a five-element Windkessel model can be used for the outlet boundary condition in coronary flow, such as the one present in figure 5.7.

In this model: R_a, R_v, $R_{a,micro}$ and $R_{v,micro}$ represent the resistance of the arterial, venous and both arterial and venous capillary levels. C_a and C_{im} are its arterial and intramyocardical compliances and p_a, p_v and p_{im} correspond to the arterial, venous and intramyocardical pressures, respectively [37] [19].

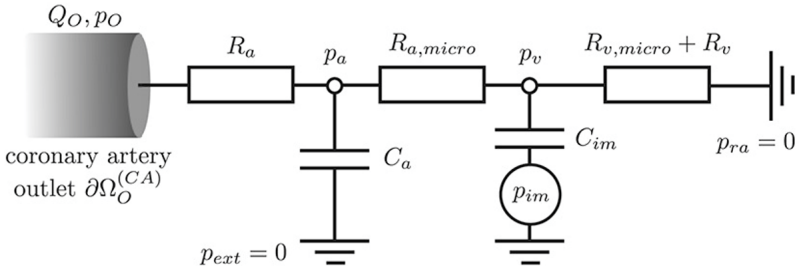

Figure 5.7: Five-element outflow boundary condition. Adapted from [19]

The governing equations of flow that we derive from this model are the following:

$$p_0 = p_a + R_a Q_0 \tag{5.39}$$

$$\frac{dp_a}{dt} = \frac{Q_0}{C_a} - \frac{p_a - p_v}{C_a R_{a,micro}} \tag{5.40}$$

$$\frac{dp_v}{dt} = \frac{dp_{im}}{dt} + \frac{1}{C_{im}}\left(\frac{p_a - p_v}{R_{a,micro}} + \frac{p_v}{R_{v,micro} + R_v}\right) \tag{5.41}$$

Jonášová and Vimmr (2021) conducted a study with different outlet models, including the

three-element and five-element Windkessel models here presented, as well as two more detailed ones, which are presented in figure 5.8:

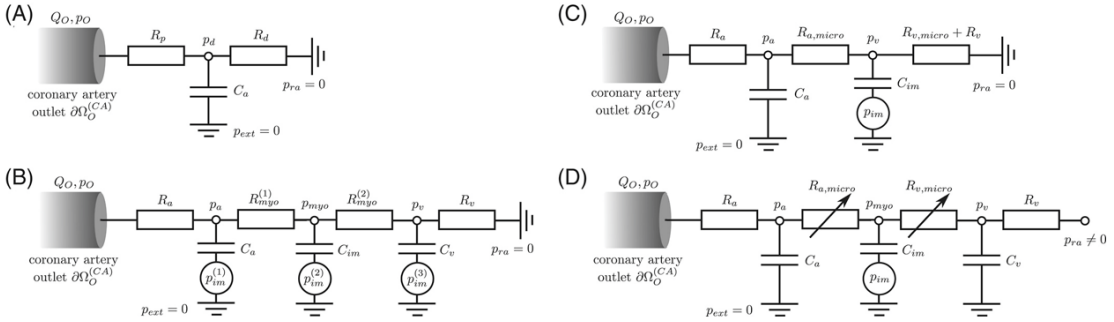

Figure 5.8: Different lumped-parameter models for coronary outflow. Adapted from [19]

Both the five-element model here presented and the more complex ones were able to represent hemodynamics as a whole in accordance to the physiological expectations, such as the delayed diastolic blood filling in coronary circulation, which the model with three-elements isn't able to accomplish. Furthermore, the five-element model obtained more adequate flow rate and shear stress results in comparison to the ones with more parameters. This, coupled with the reduced amount of parameters to estimate, made it the most promising of all and was thus utilized in this work. For more details in this analysis, the reader is encouraged to read [19].

Chapter 6

Methodology

The use of coronary computed tomography angiography (CTA) allows us to obtained image of the patients' vessels. These images can then be used to obtain patient-specific geometric models of coronary arteries. It is then possible to run hemodynamic simulations using computational fluid dynamics (CFD), which, with the increase in computational capacity, has led to an increase in research in the field.

In this chapter, the whole process used to run the hemodynamic simulations, from the CTA images and patients' data that were made available to the author, is presented: the geometry reconstruction of each patient's artery; the physiological alterations under hyperemic conditions; the implementation of the five-element Windkessel model; the mesh convergence study used to identify the most optimal one to use in the simulations; the numerical methods used in the calculations.

It is of previous note that the deformation of the vessels' walls was not taken into account, since the increase in computational cost this would provoke is too big for an insignificant improvement on the model [20].

6.1 Data of the patients in study

In this study, two patients were analyzed with stenosed LCAs and different degrees of lesion, which will be further referred to as Patient 1 and Patient 2. Patient 1 is a 63-year-old male and has a 40% stenosis located in the proximal region of the LAD. Patient 2 is a 58-year-old female with a 90% stenosis in the central third of the LAD. The CTA images and invasive measurements were obtained through collaboration with the Vila Nova de Gaia/Espinho Hospital Center (CHVNG/E).

The patients who participated in this study gave informed consent and this research was approved by the local institutional ethics committee.

To conduct this investigation, the author was given measurements of the patients' heart rate, systolic blood pressure (SBP), dyastolic blood pressure (DBP) and FFR. It is of note that both SBP and DBP were measured invasively and non-invasively, with the former being done under

hyperemic conditions and the latter in a state of rest. Furthermore, two measures of both SBP and DBP were realized invasively and three non-invasively for Patient 1, while for Patient 2 only one was made. The results of these measurements are present in table 6.1:

Table 6.1: Patients data

	Patient 1	**Patient 2**
Gender	Male	Female
Age	63	58
Heart rate $[bpm]$	59	65
$\text{SBP}_{inv}[mmHg]$	142/148	102
$\text{SBP}_{ninv}[mmHg]$	118/125/133	135
$\text{DBP}_{inv}[mmHg]$	84/83	62
$\text{DBP}_{ninv}[mmHg]$	81/88/85	67
Stenosis	40%	90%
FFR	0.93	0.58

6.2 Hyperemic physiological behaviour

The measurement of the FFR of each patient was realized in the maximum hyperemia condition, through the intravenous administration of $140\mu g/kg/min$ of adenosine, as discussed previously in chapter 2. This procedure will make changes in both vessel size and cardiac blood output, which need to be taken into account in the model for coronary circulation [45] [32] [7]:

- Mean arterial pressure decreases: $MAP_{hyp} = MAP_{rest} - 6mmHg$
- Hear rate increases: $BPM_{hyp} = BPM_{rest} + 24bpm$
- The vasodilation decreases the overall viscous resistance $\frac{R_{hyp}}{R_{rest}} = 0.24$
- Blood flow output to the LCA from the heart increases: $\frac{Q_{hyp}}{Q_{rest}} = 4.4$

6.3 Geometry model of the LCA

In order to utilize CFD in determining FFR, it is necessary to obtain a reconstruction of the artery that can be used for the calculation. In order to to this, the author made use of the CTA images given and, through available software, obtained a model that represents the LCA of each patient.

6.3.1 Geometry reconstruction in resting conditions

The CTA images of each patient were made available by the CHVNG/E in DICOM format. Through this images, the LCA was firstly reconstructed using the Mimics® software, which provides a semi-automatic method of reconstructing the lumen of the LCA.

By loading the DICOM images into the program, it presents the heart in three views (axial, coronary and sagittal), from which a series of notable points where selected: a starting one corresponding to the aorta and ending points which represent the outlets of the LCA's branches. With the selected points, the software automatically generates a 3D model of the selected domain of the LCA. The geometries obtained for both patients are present in figure 6.1.

Figure 6.1: LCA lumen models obtained with Mimics® for Patient 1 (left) and Patient 2 (right)

As can be observed, the models obtained are quite rough and don't have proper inlet and outlets, which need to be a plane sections in order to properly define boundary inflow and outflow conditions. In order to make alterations to the model that solve the mentioned problems, the software 3-matic® was utilized.

The geometry obtained in Mimics® was exported to 3-matic®. First, the surface was smoothed utilizing the *Smoothing* tool and later the *Local Smoothing* one, in the rougher areas which still needed further smoothing. After this, the trim tool was used in order to define the model's boundaries, obtaining the plane sections that correspond to the inlet and the outlets. Furthermore, the inlet of the model was centered with the Cartesian referential, using the *Sketch* tool to create a point in its center and translating it to the origin of the axis, which besides this translation makes the inlet plane have the direction of the z coordinate of the referential.

After these steps, the models for the LCA geometries were obtained under resting conditions, which are represented in figure 6.2.

6.3.2 Geometry reconstruction under maximum hyperemia

When in maximum hyperemic conditions, the vessels will dilate, which makes it necessary that the model is adapted for such conditions. This makes it necessary to estimate the increase of the cross-sectional area [45].

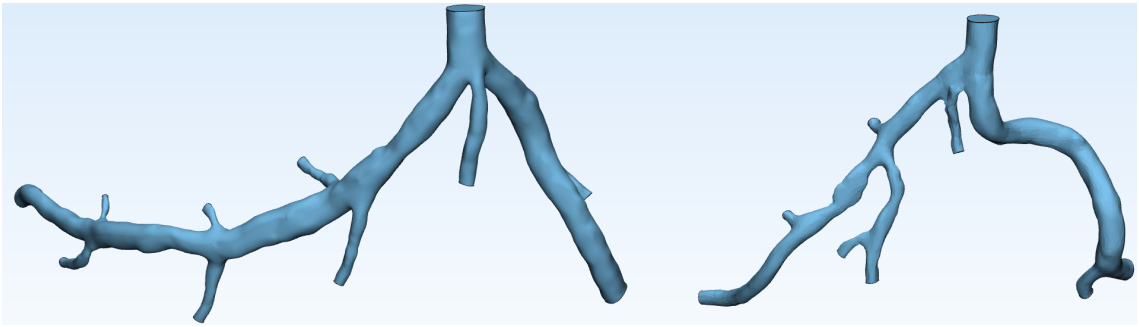

Figure 6.2: LCA lumen models obtained with 3-matic® for Patient 1 (left) and Patient 2 (right)

As seen in 6.2, under hyperemic conditions there is a defined decrease in viscous resistance. Thus, if we define a proportional relationship between sectional area and resistance, we can get the wanted alterations.

Let us consider the Hagen-Poiseuille flow's function for R:

$$R = \frac{8\eta\Delta L}{\pi R^4} \tag{6.1}$$

Assuming that, as in this case, R for coronary circulation is inversely proportional to the fourth power of of the vessel's diameter, we can obtain the increase in cross-sectional area under maximum hyperemia:

$$\frac{R_{hyp}}{R_{rest}} = \frac{r_{rest}^4}{r_{hyp}^4} = 0.24 \Leftrightarrow \frac{r_{rest}}{r_{hyp}} = \sqrt[4]{0.24} \tag{6.2}$$

Considering the cross-sectional area approximately circular, we can now arrive at the ratio between resting and hyperemic areas, since the area of a circle is given as a function of its radius by $A = \pi r^2$:

$$\frac{A_{rest}}{A_{hyp}} = \frac{r_{rest}^2}{r_{hyp}^2} = \sqrt{0.24} \Leftrightarrow \frac{A_{hyp}}{A_{rest}} = \frac{1}{\sqrt{0.24}} = 2.04 \tag{6.3}$$

Thus, it is necessary to scale the whole LCA model by 2.04 in its cross-sectional area, in order to faithfully represent the geometry under maximum hyperemia.

With this objective, the models presented in figure 6.2 were exported to the Mimics® software, so that a centerline was created utilizing the *Fit Centerline* command. This auxiliary is necessary because of the *Sectional Area* function of Mimics®, which retrieves the area of cross-sections perpendicular to the centerline created and thus to blood flow, making it possible to access each cross-sectional area of the LCA in all of the domain.

In 3-matic®, a centerline was also created, utilizing the *Create Center Line* command. Making use of it, several sketches were created in each branch, defined by a point belonging to the centerline, with it also being their normal. In each of the sketch's position, the cross-sectional area was measured in Mimics®, in manually selected approximately similar positions.

With the cross-sectional areas calculated, it is possible to arrive at the corresponding values for maximum hyperemic conditions, through the scaling factor mentioned. Considering the cross-section of each branch approximately circular, a circle was drawn in each sketch with the respectful measured area scaled by 2.04. Each circle was defined by its center being located in the centerline and a radius obtained from the equation of a circle's area: $r = \sqrt{\frac{A}{\pi}}$.

Utilizing the *Sweep-loft* command in 3-matic®, it is possible to obtain the surfaces which correspond to the dilated vessels. Such is done by defining a *Start profile*, *End profile* and *Intermediate profiles*, which correspond to the drawn circles in each vessel and a *Sweep path* which was selected to be the centerline. Having these sufaces created, in order to represent the joints of multiple branches, the *Loft* tool was utilized, with the definition of a *Start profile* and an *End profile* which correspond to the circles located at the boundaries of the surfaces created.

Though the reconstruction of the geometry is completed with these steps, the model isn't yet fit to be utilized in ANSYS®. In order to do that, first the 3-matic® *Fix wizard* was utilized, in order to solve any problems with the model, such as bad contours or overlapping triangles. After that, the geometry was exported to as an IGES file and imported into SpaceClaim®, which allows for the automatic preparation of the model by running the commands in the *Repair* column, stitching the model's different faces and solving problems related to *Split edges, Extra Edges, Missing Faces* and *Duplicates*, having an individual command for each one mentioned.

Finally, the model was exported as Parasolid text file and imported into Solidworks®, due to this format being easily read by the latter software. This operation was performed so that the file could then be exported from Solidworks® in the ACIS format, which is ideal to be utilized in ANSYS Fluent®.

After this process was completed for both cases, it was possible to obtain the models of the two patients' lumen with the vasodilation provoked under maximum hyperemia, which are presented in figure 6.3.

For a more detailed analysis of the reconstruction process, the reader is directed to [3], which utilized the same method.

It is of note that this process is highly manual and thus leads to some loss of geometrical information, which is further increased in arteries with more acute lesions. Nevertheless, with the means available, it still provides us with models that possess the main characteristics of the arteries, with a big importance being put into the stenosed region.

6.4 Rheological model for blood's viscosity

As discussed in 4.4.1, blood's viscosity was be modeled by a viscoelastic sPTT model [32]. Furthermore, it is considered to be incompressible, having constant density throughout the coronary

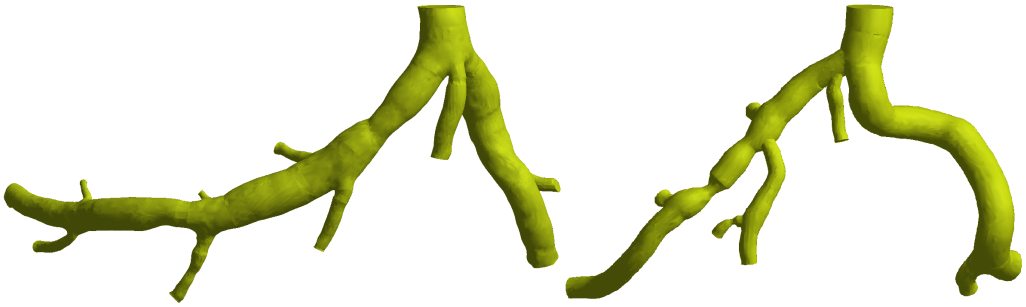

Figure 6.3: LCA lumen models under maximum hyperemic conditions for Patient 1 (left) and Patient 2 (right)

circulation: $\rho = 1060[kg/m^3]$.

The equations of the sPTT model were presented in section in 4.4.1 and the values that best fit blood behaviour for the model's coefficients were adjusted through experimentation by Deano *et al.* [8] and are presented in table 6.2, being the ones used in this work.

Table 6.2: Parameters of the sPTT model

Mode(k)	$\eta_{e_k}(Pa \cdot s)$	$\lambda_k(s)$	$\varepsilon_k()$
1	0.05	7	0.2
2	0.001	0.4	0.5
3	0.001	0.04	0.5
4	0.0016	0.006	0.5
5 (solvent)	0.0012	0	0

This model was implemented through an UDF in ANSYS Fluent®, as was developed by Pinto *et al.* [32] and coupled with the solver as blood's viscosity.

6.5 Inlet velocity boundary condition

As discussed in 3.3.3, blood circulation is a transient pulsatile flow. Thus, a womersley profile for the velocity at the model's inlet was applied, which is represented by equation 3.34.

In order to obtain the velocity profile, it is necessary to first obtain the Womersley number, which equation is again presented:

$$Wo = r\sqrt{\frac{\rho\omega}{\eta}} \tag{6.4}$$

The inlet radius, r, corresponds to inlet's circular profile radius under hyperemic conditions, which was previously defined for each patient.

In order to calculate the angular frequency, ω, it is necessary to take into account the increase in heart rate under maximum hyperemia. After it is taken into account, we can obtain it through the following equation:

$$\omega = \frac{2\pi HR_{hyp}}{60} \tag{6.5}$$

with ω being calculated in rad/s.

Though blood's viscosity is not constant, being given by the sPTT model previously presented, to calculate *Wo* we will stipulate its value to be a constant in the inlet: $\eta = 0.00345[Pa \cdot s]$.

The values of *Wo* obtained for each patient, as well as the values used to calculate it, are presented in table 6.3.

Table 6.3: Parameters for calculating *Wo*

	Patient 1	**Patient 2**
$r(mm)$	3.396	3.002
$\rho(kg/m^3)$	1060	1060
$\eta(Pa \cdot s)$	0.00345	0.00345
BPM_{rest}	59	65
BPM_{hyp}	83	89
ω	8.692	9.320
Wo	5.549	5.080

In order to obtain the time dependent velocity profile, an expansion using Fourier series was done in Matlab® by Pinho *et al.* [31]. The profile obtained was implemented in a UDF and coupled with the solver of ANSYS Fluent®, in order to be used as a boundary condition for the velocity in the inlet of each model.

The average velocity at the inlet through a cardiac cycle of Patient2 is represented in figure 6.4, for reference, since for Patient 1 the waveform is similar, just with different magnitude. It is of note that in the x axys an adimentional time is utilized, $t^* = t/T$. This is done so that the two profiles can be made more similar, since the cardiac cycle has a different duration for each patient, due to the different heart rates:

$$T = \frac{60}{HR_{hyp}} \tag{6.6}$$

which will lead to a value of $0.72[s]$ for Patient 1 and $0.67[s]$ for Patient 2.

6.6 Outlets pressure boundary condition

As the boundary condition in the outlets of the models, the five-element lumped-parameter model was utilized, as mentioned in 5.2.3. The governing equations of this model are presented again, as

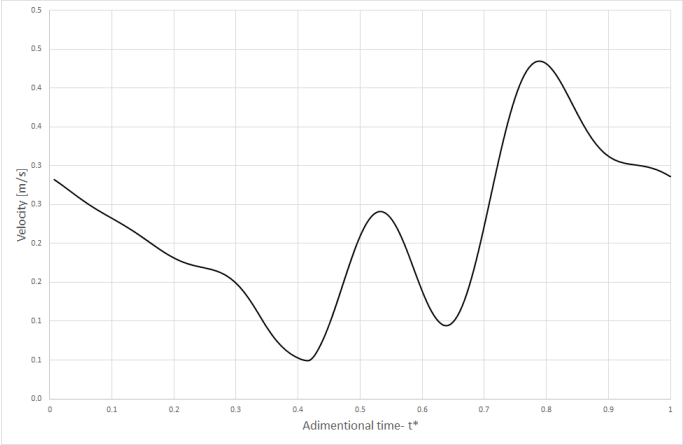

Figure 6.4: Womersley velocity profile of Patient2

a point of reference:

$$p_0 = p_a + R_a Q_0 \tag{6.7}$$

$$\frac{dp_a}{dt} = \frac{Q_0}{C_a} - \frac{p_a - p_v}{C_a R_{a,micro}} \tag{6.8}$$

$$\frac{dp_v}{dt} = \frac{dp_{im}}{dt} + \frac{1}{C_{im}}\left(\frac{p_a - p_v}{R_{a,micro}} + \frac{p_v}{R_{v,micro} + R_v}\right) \tag{6.9}$$

These equations can be further combined to reduce the system to two governing equations, now not dependent of p_a:

$$\frac{d(p_0 - R_a Q_0)}{dt} = \frac{Q_0}{Ca} - \frac{p_0 - R_a Q_0 - p_v}{C_a R_{a,micro}} \tag{6.10}$$

$$\frac{dp_v}{dt} = \frac{dp_{im}}{dt} + \frac{1}{C_{im}}\left(\frac{p_0 - R_a Q_0 - p_v}{R_{a,micro}} + \frac{p_v}{R_{v,micro} + R_v}\right) \tag{6.11}$$

This model was implemented in a UDF, in order to be used in ANSYS Fluent®. To do this, the equations need to be discretized using a second-order implicit method, which is described as follows, with ϕ being an arbitrary variable:

$$\frac{d\phi}{dt} = \frac{3\phi^{i+1} - 4\phi^{i} + \phi^{i-1}}{2\Delta t} \tag{6.12}$$

where i indicates the time-step of the calculation, with ϕ^{i+1} being the value of the variable in the next time step and ϕ^{i-1} the same value in the previous time step. Δt represents the chosen duration for each time-step of the calculation.

Applying this formulation to the differential governing equations, we can develop them and

obtain the following result:

$$\left(\frac{3}{2}\frac{C_a}{\Delta t}+\frac{1}{R_{a,micro}}\right)p_0^{i+1} = Q_0^{i+1}-C_a\frac{-4p_0^i+p_0^{i-1}}{2\Delta t}+R_aC_a\frac{3Q_0^{i+1}-4Q_0^i+Q_0^{i-1}}{2\Delta t}+\frac{R_a}{R_m}Q_0^{i+1}+\frac{p_m^{i+1}}{R_m}$$

$$\left(\frac{3}{2}\frac{C_m}{\Delta t}+\frac{1}{R_m}+\frac{1}{R_{v,micro}+R_v}\right)p_m^{i+1} = C_m\left(\frac{3p_{im}^{i+1}-4p_{im}^i+p_{im}^{i-1}}{2\Delta t}-\frac{-4p_m^i+p_m^{(}i-1)}{2\Delta t}\right)\frac{p_0^{i+1}}{R_m}-\frac{R_a}{R_m}Q_0^{i+1}+\frac{p_{out}}{R_{v,micro}+R_v}$$

The UDF cannot solve this system of equations, since it reads and compiles one line of code at a time, not being able to join both equations and find a result. Thus, this system must be developed in order to update the value of p_0 in each iteration, which corresponds to the average pressure in the outlet. The following equations were inserted in an UDF in order to implement the model in ANSYS Fluent®:

$$\frac{dq}{dt} = \frac{3Q_0^{i+1}-4Q_0^i+Q_0^{i-1}}{2\Delta t} \tag{6.13}$$

$$\frac{dp_{im}}{dt} = \frac{3p_{im}^{i+1}-4p_{im}^i+p_{im}^{i-1}}{2\Delta t} \tag{6.14}$$

$$aux = \frac{3C_m}{2\Delta t}+\frac{1}{R_m}+\frac{1}{R_{v,micro}+R_v} \tag{6.15}$$

$$p_0^{i+1} = \left[\left(1+\frac{R_a}{R_m}\right)Q_0^{i+1}+C_a\left(R_a dq-\frac{-4p_0^i+p_0^{i-1}}{2\Delta t}\right)\right]/\left(\frac{3C_a}{2\Delta t}+\frac{1}{R_m}-\frac{1}{auxR_m{}^2}\right) \tag{6.16}$$

$$p_v^{i+1} = \frac{1}{aux}\left(\frac{p_0^{i+1}}{R_m}+C_m\left(dp_{im}-\frac{-4p_v^i+p_v^{i-1}}{2\Delta t}\right)-\frac{R_a}{R_m}Q_0^{i+1}+\frac{p_{out}}{R_{v,micro}+R_v}\right) \tag{6.17}$$

where aux is an auxiliary variable used to simplify the equations.

6.6.1 Patient-specific lumped parameters

As stated before, this model can only produce results in determining FFR if its parameters are well adjusted to each specific patient.

The intra myocardical pressure can be considered to be approximately equal to the pressure in the left ventricle, which is represented in figure 6.5.

This pressure was estimated as being 0 in the dyastole and equal to the aortic pressure, which is the pressure at the inlet of the model, during systole, neglecting the increasing and decreasing pressure in transition between these two phases of the cardiac cycle:

$$p_{im} = \begin{cases} 0, & 0.38 < \frac{t}{T} < 0.61 \\ p_{inlet}, & otherwise \end{cases} \tag{6.18}$$

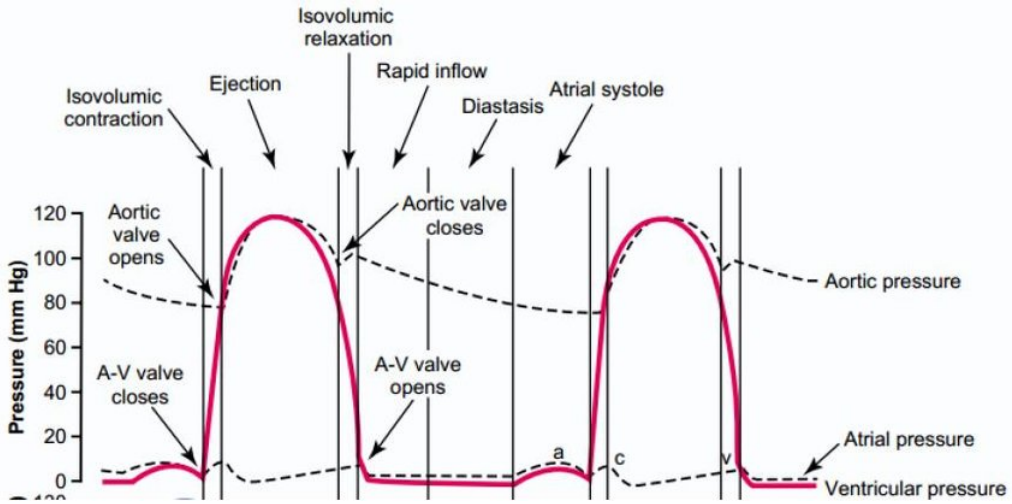

Figure 6.5: Aortic, atrial and left ventricular pressure

with p_{inlet} being calculated with ANSYS Fluent® through the same UDF for each iteration as the average pressure in the surface.

The total resistance to flow, which involves both the arterial and venous circulation, was determined by the average pressure divided by the average flow rate in the inlet:

$$R_{total} = \frac{MAP}{Q_{avg}} \tag{6.19}$$

$$MAP = DBP + \left[\frac{1}{3}(HR \cdot 0.0012)\right](SBP - DBP) \tag{6.20}$$

where MAP is the mean arterial pressure, SBP and DBP are the diastolic and systolic pressures that were measured and HR is the heart rate. Q_{avg} was determined as the average of the Womersley velocity profile imposed as the boundary condition in the inlet, for each patient.

The values of R_{total} and the parameters utilized to calculate them for each patient are present in table 6.4.

Table 6.4: Parameters for calculating *Wo*

	Patient 1	**Patient 2**
Q_{avg}	3.396	3.002
SBP	145	102
DBP	83.5	62
HR	0.983	1.083
MAP	104	75
R_{total}	10.2×10^6	7.36×10^6

As we can see, R is inversely proportional to the flow rate. We can thus assign a value of R for each outlet as a fraction of the total value, in terms of its area:

$$R_i = R_{total}\frac{A_i}{\sum_{i=1}^{N} A_i} \tag{6.21}$$

where i is the number indicating the outlet in question and N is the number of outlets of the model.

The resistance in the venous circulation can be obtained through the same principle, considering an average pressure in the venous vessels of $20 mmHg$:

$$R_v, i + R_{v,micro,i} = 20 \cdot 133.32\frac{A_i}{\sum_{i=1}^{N} A_i} \tag{6.22}$$

where 133.32 is used to convert the venous pressure to *Pascal*.

The arterial resistance can be calculated through the following equation:

$$R_{a,i} = \frac{\rho c_i}{A_i} \tag{6.23}$$

$$c_i = \sqrt{\frac{2}{3\rho}\left(k_1 e^{k_2 R_i} + k_3\right)} \tag{6.24}$$

where $\rho = 1060\left[kg/m^3\right]$ is blood's density, c_i is the pulse wave velocity, R_i is the radius of the outlet and the k constants are given as follows:

$$k_1 = 2 \cdot 10^7\left[g^2 s^{-1} cm^{-1}\right] \tag{6.25}$$

$$k_2 = -22.53\left[cm^{-1}\right] \tag{6.26}$$

$$k_3 = 8.65 \cdot 10^5\left[g^2 s^{-1} cm^{-1}\right] \tag{6.27}$$

Having both the total and venous and systemic arterial resistances been calculated, the arterial microcirculation resistance can be obtained simply through difference between these values:

$$R_{a,micro,i} = R_{total,i} - (R_{v,i} + R_{v,micro,i}) - R_{a,i} \tag{6.28}$$

we then obtain the components of the circulatory resistance for each outlet of the models, which are represented in table 6.5 an 6.6, for Patients 1 and 2, respectively.

Both arterial and intra-myocardical capacitances were prescribed to have physiological meaning as a function of the patients myocardial mass:

Table 6.5: Resistances- Patient 1

$Area \times 10^6[m^2]$	$(R_v + R_{v,micro}) \times 10^{-4}\left[Pa \cdot s/m^3\right]$	$R_a \times 10^{-8}\left[Pa \cdot s/m^3\right]$	$R_{a,micro} \times 10^{10}\left[Pa \cdot s/m^3\right]$
2.97	4.13	1.58	1.47
16.60	0.74	0.28	8.29
4.99	2.46	0.94	2.48
2.80	4.37	1.67	1.38
2.38	5.15	1.97	1.17
0.58	21.24	8.11	0.21
3.36	3.65	1.39	1.66
0.85	14.43	5.51	0.37
2.29	5.35	2.04	1.12
9.17	1.34	0.51	4.57

$$C_a = 0.013\left[ml \cdot mmHg^{-1}100g_{myo}^{-1}\right] \tag{6.29}$$

$$C_{im} = 0.254\left[ml \cdot mmHg^{-1}100g_{myo}^{-1}\right] \tag{6.30}$$

since access to the patient's myocardial mass wasn't made available, an average value of $100[g]$ was prescribed. In order to see if a wrong assumption of this value would produce misleading results, an analysis of the model sensitivity to such variations was done, with simulations being done for values of myocardial mass of $60[g]$, $100[g]$ and $140[g]$.

Finally, intramyocardical pressure, p_{im},was set to $5mmHg$, which makes all the parameters estimated for each patient [7].

6.7 FFR quantification

As stated in the introduction to this work, the current standard practice utilized to determine the FFR of a patient is the measurement of the aortic and distal pressures in relationship to the lesion.

$$FFR = \frac{p_{distal}}{p_{aortic}} \tag{6.31}$$

These measurements are in good practice realized at distances of $10mm$ and $20mm$ of the coronary tree inlet and the stenosis location, respectively.

In order to obtain this values, during blood flow simulation, two planes were created for each patient in ANSYS Fluent®, corresponding to the aortic and distal locations. These planes were defined using the centerlines that were created in 3-matic®, corresponding to their direction. Furthermore, the aortic plane was considered to be the entrance pf the model, distancing $2.5mm$ from the inlet, while the distal plane distances $20mm$ upstream from the lesion, in the LAD. The aortic plane location was estimated, since the inlet of our model is at an unknown distance of the

Table 6.6: Resistances- Patient 2

$Area \times 10^6 [m^2]$	$(R_v + R_{v,micro}) \times 10^{-4} \left[Pa \cdot s/m^3\right]$	$R_a \times 10^{-8} \left[Pa \cdot s/m^3\right]$	$R_{a,micro} \times 10^{10} \left[Pa \cdot s/m^3\right]$
14.1	0.80	0.19	6.33
5.02	2.25	0.54	2.25
2.55	4.41	1.06	1.14
4.44	2.54	0.61	1.99
3.49	3.23	0.78	1.56
1.76	6.39	1.53	0.78
4.61	2.44	0.59	2.07
6.3	1.79	0.43	2.83

coronary tree's entrance, but it should provide a good estimation since blood flow until the first branches is pretty stable. The resulting planes are present in figure 6.6.

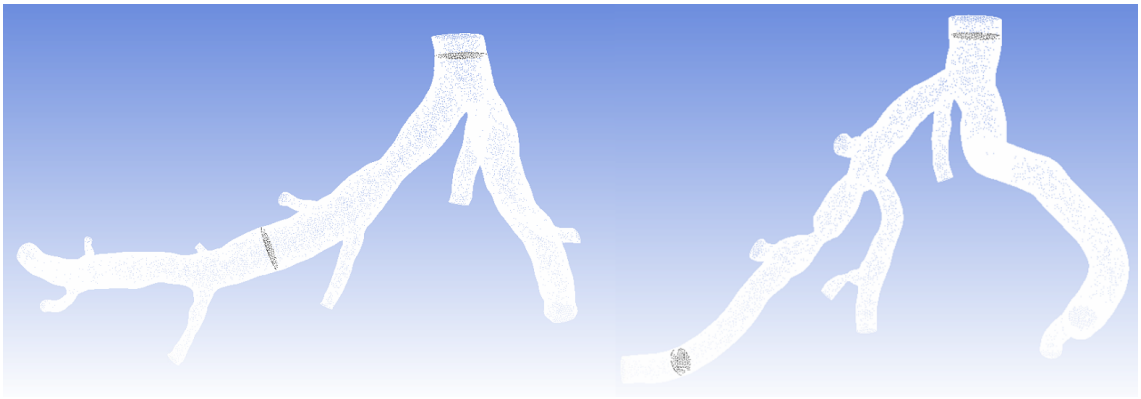

Figure 6.6: Aortic and distal planes for Patient 1 (left) and Patient 2 (right)

Having defined both planes, ANSYS Fluent® is able to calculate the average relative total pressure in both of them for each time step of calculation. This is done by the quotient of the sum of the pressure in all cell faces that are located in the planes, multiplied by their area, and the total area of the vessel's section in each plane. It is then possible to obtain the average distal and aortic pressures through each cycle, by using the trapezoid rule, which gives a second-order approximation of the value of an integral:

$$p_{avg} = \frac{1}{T}\int_0^T p dt = \frac{\Delta t}{2T}\left(p_0 + 2p_1 + \ldots + 2p_{n-1} + p_n\right) \tag{6.32}$$

where Δt is the calculation time-step, which was defined as $0.005s$ and $n = \frac{T}{\Delta t}$ is the number of values obtained.

6.8 Mesh selection

In CFD, the quality of the results obtained is highly dependent on the quality of the mesh that is applied. A course mesh leads to inaccurate calculus, jeopardizing the results obtained while meshes that are unnecessarily fine lead to very large computational times without need.

The models' meshes were created wth the ANSYS Meshing™ tool. The Thetrahedrons method was chosen, with the options of patch independent mesh and no refinement being chosen, making the mesh uniform across the model. The maximum size of the elements is the parameter that must be analyzed in order to obtain the most optimal mesh for each model.

In order to balance both these factors, an analysis of successive finer meshes was done, having the average pressure in the distal plane during one cardiac cycle been utilized to determine the degree of convergence in the calculation. Furthermore, the parameter *Skewness*, which is utilized to evaluate mesh quality in ANSYS®, was obtained. This parameter must always be smaller than 0.95, in order to obtain stable and convergent calculus.

The model produces an anomaly in the beginning of the first cardiac cycle, due to the initialization of the parameters. Thus, all calculations will be done for the second cardiac cycle, the mesh analysis being one of them.

The parameters of each mesh are present in tables 6.7 and 6.8, as well as the maximum and average *Skewness*.

Table 6.7: Meshes parameters- Patient 1

	Max. element size	**Nr. of elements**	**Max Skewness**	Avg. Skewness
Mesh 1	6.7×10^{-4}	126568	0.754	0.154
Mesh 2	5.3×10^{-4}	255996	0.867	0.136
Mesh 3	4.22×10^{-4}	507641	0.6840	0.125

Table 6.8: Meshes parameters- Patient 2

	Max. element size	**Nr. of elements**	**Max Skewness**	**Avg. Skewness**
Mesh 1	6.7×10^{-4}	74013	0.880	0.168
Mesh 2	5.3×10^{-4}	149715	0.879	0.150
Mesh 3	4.22×10^{-4}	295555	0.881	0.147

In order to analyze the degree of convergence in the results, the Richards Interpolation method was utilized. Considering p_{avg} as the average pressure in the distal plane and 1 and 2 as referring to a coarser and finer mesh, by having the results of p_{avg} calculated with mesh 1 and 2, we can estimate its real value through the following equation, considering a second order solution:

$$p_{avg} = p_1 + \frac{p_1 - p_2}{r^2 - 1} \tag{6.33}$$

$$r = \frac{h_2}{h_1} \tag{6.34}$$

with p_1 and p_2 being the pressure values obtained with meshes 1 and 2 and h represents the cell size of the meshes.

We can thus obtain the approximate real value of p_{max} by using the two finer meshes considered and calculate the relative error that each mesh produces in relationship:

$$e_r = \frac{p_{avg} - p_i}{p_{avg}} \cdot 100 \tag{6.35}$$

where i is the mesh in analysis.

With this procedure, we obtain the following value for the approximation of p_{avg}

$$r = \frac{h_4}{h_3} \tag{6.36}$$

$$p_{avg} = \frac{p_3 - p_4}{r^2 - 1} \tag{6.37}$$

The results for each mesh in terms of relative error are presented in table 6.9, from which we can see that mesh 3 improves the result of mesh 2 for a very small margin, for both patients, which isn't worth the increment in computational time. Mesh 2 was thus utilized in this work for all blood flow simulations.

Table 6.9: Meshes parameters- Patient 2

$e_r[\%]$	**Mesh 1**	**Mesh 2**	**Mesh 3**
Patient 1	4.010	1.345	0.350
Patient 2	3.427	1.078	0.277

6.9 Calculation methods

In order to solve the governing equations, the SIMPLE algorithm was utilized. In the time formulation for the resolution of the pressure and flow fields, as well as for the five-element Windkessel model boundary condition in the outlets, a second order implicit scheme was used. As for the scalars introduced by the use of the viscoelastic non-Newtonian sPTT model for blood, a second order upwind discretization scheme was used.

The time step chosen was of $0.005s$, $\Delta t = 0.005s$, with 20 iterations per time step. The results for the hemodynamic simulations were saved every $0.02s$, apart from the pressure in the aortic and distal planes and the outlets, which were saved every time-step. The convergence criteria for the continuity and momentum equations, as well as for the scalars of the sPTT model, was of 1×10^{-6}.

Chapter 7

Results and discussion

In this chapter, the FFR values obtained through hemodynamic simulations of coronary flow for both patients 1 and 2 are compared to the values obtained invasively. The geometric model of the patient's LCA, under maximum hyperemia, are analyzed for the three different scenarios of the tuning of the lumped parameters of the five-element Windkessel model.

The model's sensitivity is also studied when it comes to the compliance, which is dependent on the patients' myocardial mass, and the duration of the systole. Both these characteristics are studied by the change in their value for Patient 2, in order to find the influence they have in FFR calculus.

Apart from the FFR calculus, the pressure and velocity fields across the model are analyzed, as well as the average pressure in the outlets, in order to make a viable conclusion about the parameters that were used.

7.1 Velocity fields

In this section, the velocity wave forms for both patients, which were obtained through the Ansys tool CFD Post®, are presented. By analyzing figure 6.4, we can see that the velocity fields have a maximum and a minimum, which correspond to $t^* = \frac{t}{T} = 0.79$ and $t^* = \frac{t}{T} = 0.425$. The velocity waveforms of both patients in these instants of the cardiac cycle are presented in figures 7.1 and 7.2.

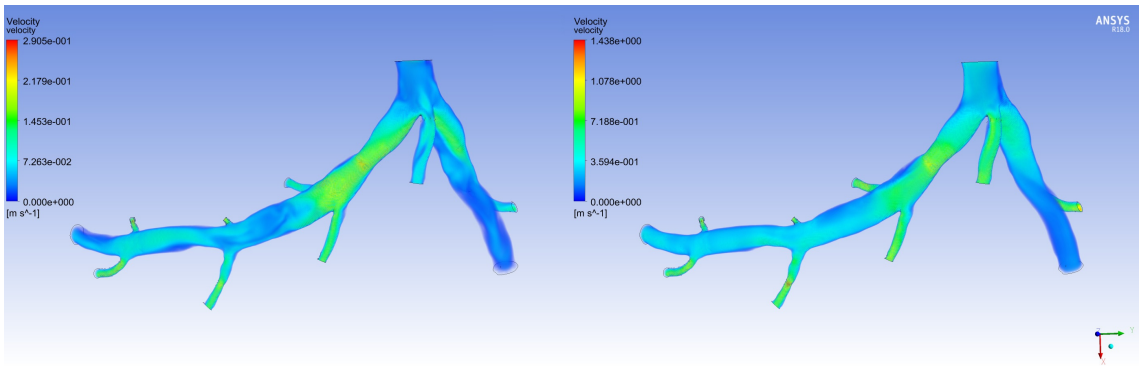

Figure 7.1: Velocity fields of Patient 1 for the minimum (left) and maximum (right) average velocities

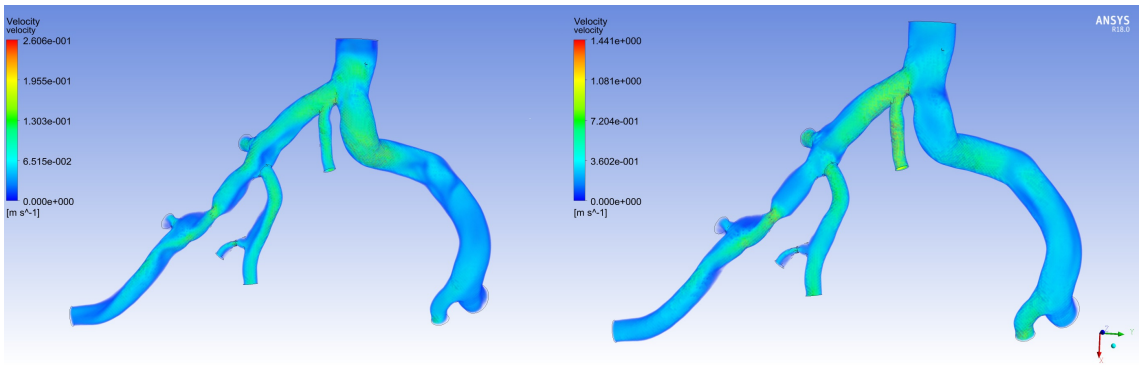

Figure 7.2: Velocity fields of Patient 2 for the minimum (left) and maximum (right) average velocities

We can identify clearly that areas with a thinner section have higher velocity magnitudes, which is expected due to the increase in dynamic pressure. Although there is a velocity reduction due to friction losses, this is the most predominant factor, with velocity being higher downstream rather than in the inlet due to the vessels getting progressively thinner.

7.2 Pressure fields

In order to better understand the development of coronary blood flow, the pressure fields across the models are represented in this section. The results are gathered in the same instant of the cardiac and through the same software as the velocity fields, and are present in figures 7.3 and 7.4.

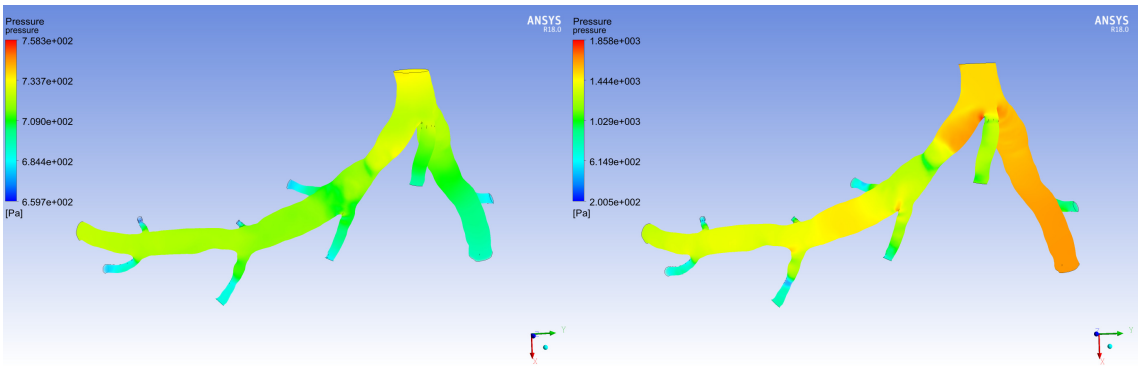

Figure 7.3: Pressure fields of Patient 1 for the minimum (left) and maximum (right) average velocities

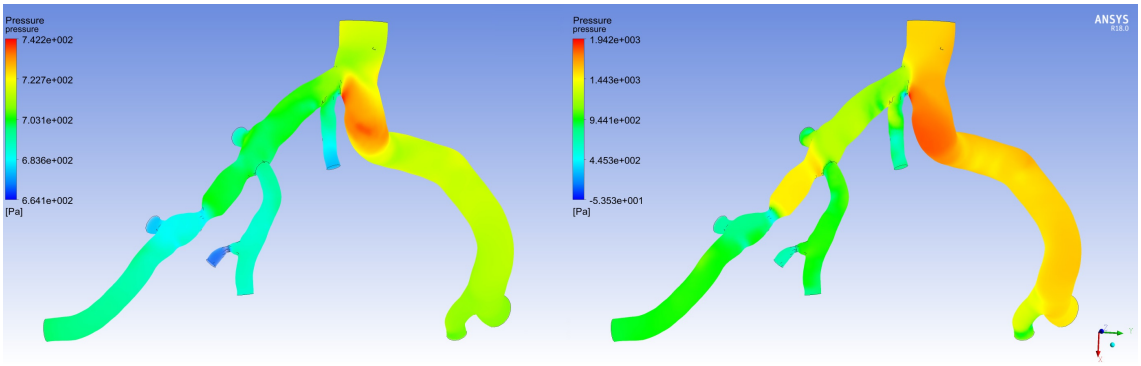

Figure 7.4: Pressure fields of Patient 2 for the minimum (left) and maximum (right) average velocities

In these models, we can very distinctly see the effect of the stenosis, since the branches that have been formed before its locations manage to maintain a higher pressure value than those which are affected by it. We can also see that for Patient 2, since the stenosis is way more acute, the pressure reduction that is provoked by it is much bigger than that of Patient 1. Furthermore, opposite to what happens with velocity, in the thinner vessels the pressure tends to be smaller, due to larger predominance of viscous stresses.

It is important to note that CFD Post® takes stagnation pressure into consideration, and thus doesn't take dynamic pressure into account. This is well noted due to the fact that pressure is much lower in the stenosed region and increases in the downstream area, due to the progressive decrease in velocity after the acceleration due to the thinner sections of the vessels.

7.3 Pressure waves in the models' outlets

In this section, the waveforms representing the evolution of the average pressure through a cardiac cycle in each of the models' outlets are represented in figures 7.5 and 7.6.

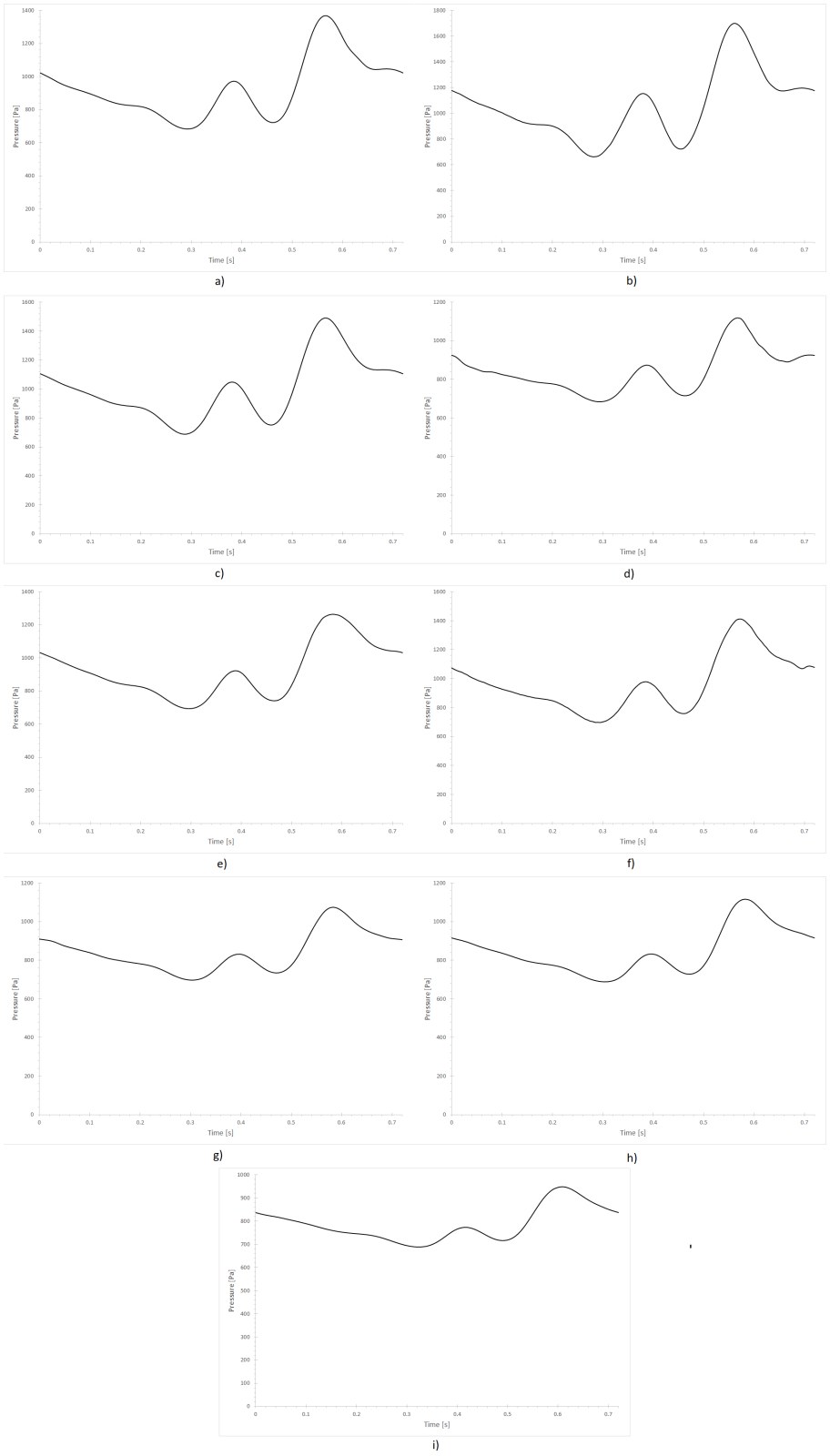

Figure 7.5: Pressure waveforms of Patient 1 for outlets: a) 1; b) 2; c) 3; d) 4; e)5; f) 6; g)7; h) 8; i) 9

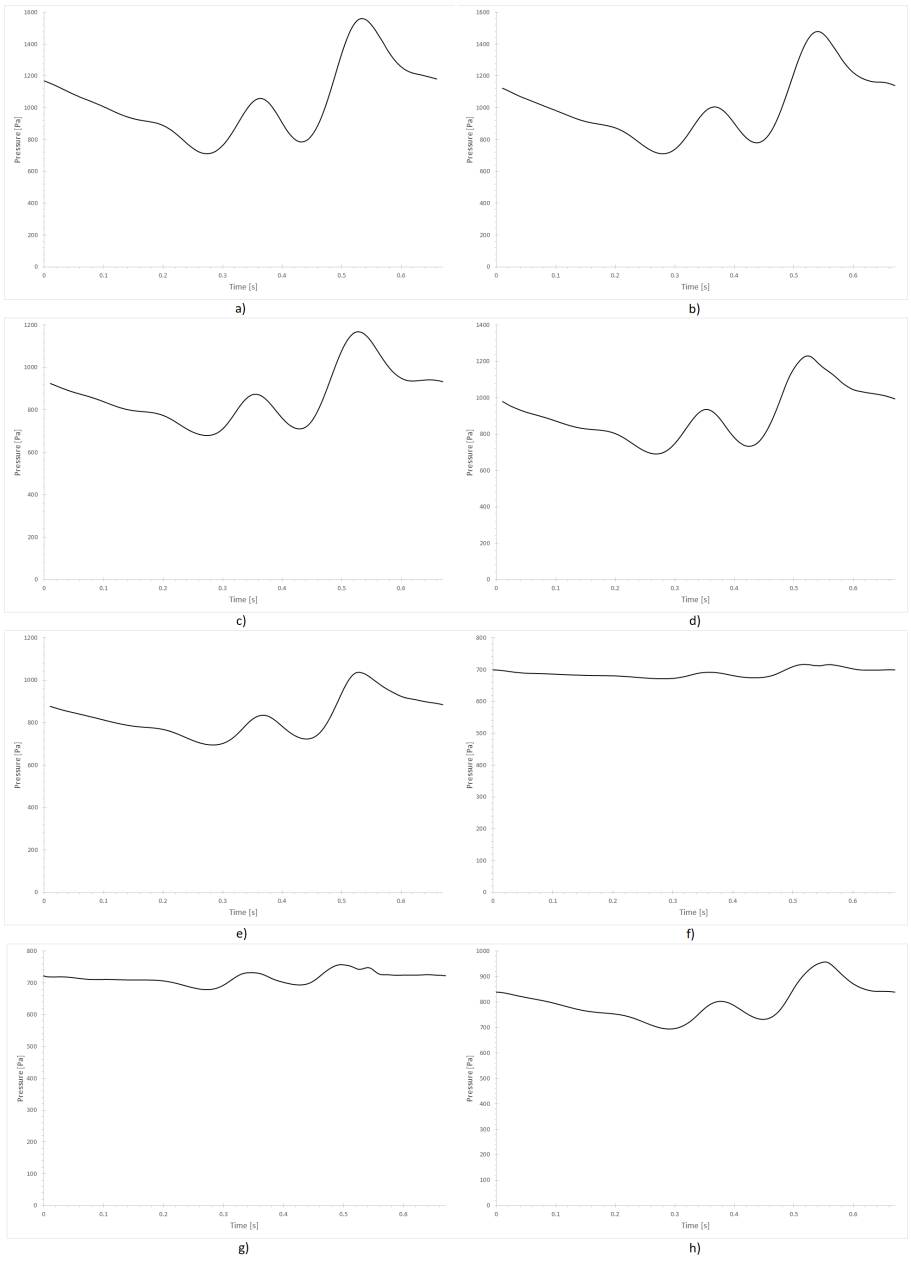

Figure 7.6: Pressure waveforms of Patient 2 for outlets: a) 1; b) 2; c) 3; d) 4; e)5; f) 6; g)7; h) 8

7.4 Computed Fractional Flow Reserve values obtained

The FFR was obtained for both patients, as the ratio between distal and aortic pressures, with the average relative total pressure being used. The average pressure waveforms for both patients in these two sections is presented in figure 7.7. It is of note that these were the profiles obtained considering $100g$ of feeding myocardial mass, with the sensitivity of the models to this parameter being discussed later.

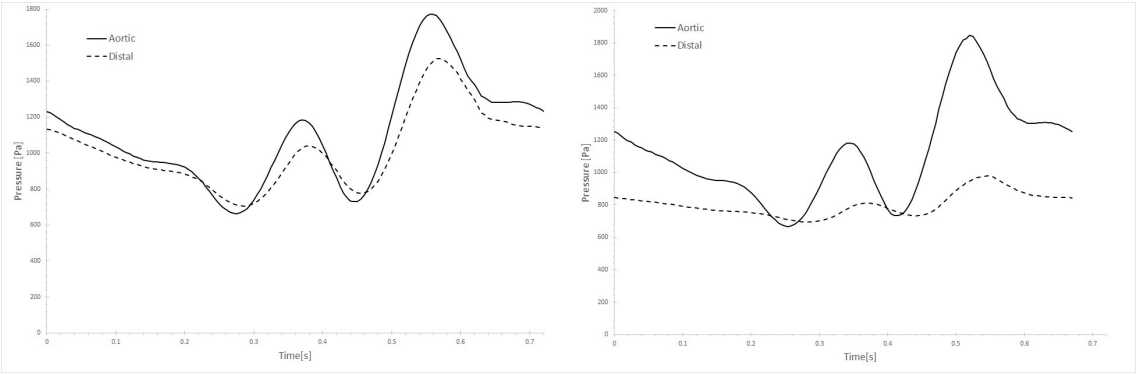

Figure 7.7: Pressure waveforms of Patient 1 (left) and Patient 2(right) in the distal and aortic planes

It is immediately noticeable the much larger decrease in pressure for Patient 2, which was expected due to the much more accentuated lesion and the smaller FFR value obtained invasively. We can also identify that the waveforms have a lag between them, which is caused by the propagation of the pressure pulse from the inlet into the branches of the coronary tree.

In table 7.1, the FFR values obtained for each patient are presented, as well as the ones obtained through the invasive method, for comparison. The relative error of the computed calculation is also present, which was calculated through the following equation:

$$e_r[\%] = \frac{\left|FFR_{computed} - FFR_{invasive}\right|}{FFR_{invasive}} \times 100 \tag{7.1}$$

Table 7.1: FFR values obtained

	Patient 1	**Patient 2**
Invasive FFR	0.93	0.58
Computed FFR	0.925	0.719
$e_r[\%]$	0.53	24

Firstly, we can identify that the lesion of Patient 1 is determined to be not significant with both methods, while the opposite is true for Patient 2, since the threshold for a lesion to be considered in need of revascularization is $FFR = 0.75$. Furthermore, we can see that the computed value obtained for Patient 1 is very similar to the invasive FFR obtained, with a negligible error, which indicates that the model used described the hemodynamics of the patient's LCA almost perfectly. In the case of patient 2, the relative error $e_r = 24\%$ indicates that the model couldn't predict the magnitude of pressure losses in flow from the aortic to the distal plane which, although in these case the model predicts the need for intervention in the artery, could be troublesome for cases with FFR values closer to 0.75.

In order to establish the model's sensibility to a variation in the Compliance, the FFR was computed for different values of myocardial mass, since it will depend on it proportionally. The values obtained are presented in table 7.2.

Table 7.2: FFR computed values for different myocardial masses

$m_{myo}[g]$	**Patient 1**	**Patient 2**
100	0.9250	0.7190
140	0.9257	0.7192
60	0.9254	0.7188

We can see that the model is virtually unaffected by these changes and thus, the estimation of $100g$ for the myocardial mass can be used as a good reference.

Chapter 8

Conclusions

In this work, two patient-specific geometry of the left coronary artery (LCA) were generated in order to perform hemodynamic simulations using computational fluid dynamics (CFD), with the objective of calculating the value of the Fractional Flow Reserve (FFR). This parameter is considered the gold standard in assessing the severity of a lesion due to stenosis and the possible need for revascularization. The computed FFR values obtained were compared with the invasively measured FFR obtained by the Vila Nova de Gaia/Espinho Hospital Center (CHVNG/E) for two patients with different levels of stenosis, in order to assess how accurate the model is when compared to invasive measuring methods.

The geometry of the patients' LCA was modeled through computed tomography angiography images (CTA) that were provided by the CHVNG/E. Through the use of the softwares Mimics® and 3-matic®, the geometry under resting conditions was reconstructed and delimited from the CTA images and then scaled by a factor of 2.04 of the cross sectional area to represent the patients' geometries in hyperemic conditions.

In order to properly simulate coronary blood flow, the geometry was loaded into ANSYS® and a mesh was created for each patient utilizing Ansys Meshing™ tool. A patient-specific Womersley velocity profile was used as the velocity boundary condition in the inlets. A simplified Phan-Thien/Tanner rheological model was implemented to model blood's viscoelastic properties. Furthermore, a patient-specific five-element Windkessel model was implemented as the pressure boundary condition for the outlets of the models, with all these models being developed as user defined functions (UDF) and implemented in Ansys Fluent®.

The Windkessel model is composed of five elements: arterial resistance (R_a), arterial microcirculation resistance ($R_{a,micro}$), venous resistance ($R_v + R_{v,micro}$), arterial compliance (C_a) and intra-myocardial compliance (C_{im}). These elements were estimated in order to produce realistic properties of coronary blood flow. The arterial resistance was obtained by approximating the pulse wave velocity and the venous resistance was estimated by considering an average venous pressure of $20 mmHg$. The compliances of the model were considered as depending on the myocardial mass

of each patient, with an average value of $100g$ being considered. In order to evaluate the error that this consideration for the compliances could provoke, an analysis of the alterations on the models produced by considering mass values of $60g$ and $140g$ was conducted.

Patient 1 has a 40% stenosed region in the proximal region of the left anterior descending artery (LAD) and Patient2 has a 90% stenosis in the medium third of the LAD. The first is considered as an intermediate lesion, while the latter is a severe one. The CHVNG/E reported FFR values measured invasively of 0.93 for Patient 1and 0.59 for Patient 2. A lesion is considered to be in need of intervention for values of $FFR < 0.75$ and hemodynamically irrelevant for values of $FFR > 0.8$. The models implemented for both patients produced FFR values of 0.925 for Patient 1, which corresponds to a relative error of $e_r = 0.53\%$, and a value of 0.719 for Patient 2, corresponding to $e_r = 24\%$. When changing the values of the compliances, as described before, virtually no change was detected in the FFR values obtained, which made it clear that the model has very low sensibility to these changes and thus the assumption of $100g$ of feeding myocardial mass can be utilized.

From the results obtained, we can see that the model holds up very well for arteries with small lesions, while it lacks in accuracy for more accentuated stenosed areas. In the author's opinion, this is due to the inability to correctly represent the geometry of the stenosed arteries when more acute lesions occur, under hyperemic conditions. Since the process of scaling the model is very manual, loss in details regarding the patient geometry are present and will be much more relevant for higher stenosis values, which clearly produces inaccurate results when obtaining the computed FFR values.

The model accurately predicted a necessity of revascularization for Patient 2 and the absence of hemodinamycally relevant stenosis for Patient1. Despite this, if the stenosis was closer to the threshold 0.75% value, the diagnostic produced could lead to erroneous conclusions.

8.1 Further Works

The developed Windkessel model shows promising results in modelling coronary blood flow. In order for it to be applied more generally for clinical practice, a development is needed in the computational reconstruction of the vessels' lumen, since it is held back by the inability to represent the geometry of the stenosed artery under hyperemic conditions in more detailed. This proccess is still highly manual and research in making this procces more automatic and precise would be the biggest improvement in the computed calculus of FFR.

Furthermore, a statistic study could be developed for many patient-specific cases in order to further study the boundaries that the model has in determining the need for revascularization of a patient, since only two cases were studied and none of them corresponded to an FFR value measured invasively that was close to the limit value of 0.75 for a lesion to be considered relevant. If, in the future, the model can be tested in more than 30 patients and the results are a good representation of the FFR values obtained through invasive measurements, it could start being used in clinical practice, reducing health risks for the patient.

References

[1] AMBOSS. Cardiac physiology. https://next.amboss.com/us/article/zo0reSrpcfIW0, september 2021.

[2] AMBOSS. Heart. https://next.amboss.com/us/article/Up0bKSj9c$_M$e0, *january*2022.

[3] A.C.M. André. *Hemodynamic simulations in a stenosed left coronary artery - FFR quantification using a Windkessel model*. PhD thesis, Faculdade de Engenharia da Universidade do Porto, Rua Dr. Roberto Frias s/n, Porto, 2021.

[4] Rick Ash, David A. Morton, and Sheryl A. Scott. *Histology: The Big Picture*. The McGraw-Hill Companies, 2013.

[5] Charles A.Taylor, Timothy A.Fonte, and James K.Min. Computational fluid dynamics applied to cardiac computed tomography for noninvasive quantification of fractional flow reserve: Scientific basis. *Journal of the American College of Cardiology*, pages 2233–2241, june 2013.

[6] Nathan Betteridge and Fiona Armstrong. Cardiac output monitoring. *Anaesthesia Intensive Care Medicine*, 23(2):101–110, 2022.

[7] Etienne Boileau, Sanjay Pant, Carl Roobottom, Igor Sazonov, Jingjing Deng, Xianghua Xie, and Perumal Nithiarasu. Estimating the accuracy of a reduced-order model for the calculation of fractional flow reserve (ffr). *International Journal for Numerical Methods in Biomedical Engineering*, 34(1):e2908, 2018.

[8] Campo-Deaño, Roel P. A. Dullens, Dirk G. A. L. Aarts, Fernando T. Pinho, and Mónica S. N. Oliveira. Viscoelasticity of blood and viscoelastic blood analogues for use in polydymethylsiloxane in vitro models of the circulatory system. *Biomicrofluidics*, 7:034102, may 2013.

[9] Marianne Catanho, Mridu Sinha, and Varsha Vijayan. Model of aortic blood flow using the windkessel effect. *University of California of San Diago, San Diago*, 2012.

[10] Jonathan C. Cohen. Genetic approaches to coronary heart disease. *Journal of the American College of Cardiology*, pages A10–A14, october 2006.

[11] Franz-Josef Neumann et al. 2018 esc/eacts guidelines on myocardial revascularization. *European Heart Journal*, pages 87—165, 2019.

[12] Gabor G.Toth et al. Standardization of fractional flow reserve measurements. *Journal of the American College of Cardiology*, pages 742–753, august 2016.

[13] Jenni Aittokallio et al. Polygenic risk scores for predicting adverse outcomes after coronary revascularization. *The American Journal of Cardiology*, january 2022.

[14] European Heart Network European Society of Cardiology. European heart health charter, june 2007.

[15] John Furst. What is the function of veins in the circulatory system? https://www.firstaidforfree.com/what-is-the-function-of-veins-in-the-circulatory-system/, may 2020.

[16] John E. Hall and Michael E. Hall. *Guyton and Hall Textbook OF Medical Physiology, Fourteenth Edition*. Elsevier, 2021.

[17] Shannan K. Hamlin and Penelope S. Benedik. Basic concepts of hemorheology in microvascular hemodynamics. *Critical Care Nursing Clinics of North America*, 26(3):337–344, 2014.

[18] Rebekka Vibjerg Jensen, Marie Vognstoft Hjortbak, and Hans Erik Bøtker. Ischemic heart disease: An update. *Seminars in Nuclear Medicine*, pages 195–207, may 2020.

[19] Alena Jonášová and Jan Vimmr. On the relevance of boundary conditions and viscosity models in blood flow simulations in patient-specific aorto-coronary bypass models. *International Journal for Numerical Methods in Biomedical Engineering*, 37(4):e3439, 2021.

[20] E Miranda, LC Sousa, CC António, CF Castro, and SIS Pinto. Role of the left coronary artery geometry configuration in atherosusceptibility: Cfd simulations considering sptt model for blood. *Computer Methods in Biomechanics and Biomedical Engineering*, 24(13):1488–1503, 2021.

[21] N Mittal, Yf Zhou, C Linares, Sophorn Ung, B Kaimovitz, Sabee Molloi, and G Kassab. Analysis of blood flow in the entire coronary arterial tree. *American journal of physiology. Heart and circulatory physiology*, 289:H439–46, 08 2005.

[22] Faith A. Morrison. *Understanding rheology*. Oxford University Press, 2001.

[23] Bruce R. Munson, Donald F. Young, and Theodore H. Okiishi. *Fundamentals of Fluid Mechanics, Fifth Edition*. John Wiley Sons, 2006.

[24] Cecil D. Murray. The physiological principle of minimum work. *Proceedings of the National Academy of Sciences*, 12(3):207–214, 1926.

[25] Abraham Noordergraaf. *Circulatory System Dynamics, Volume 1*. Academic Press, 1978.

[26] World Health Organisation. Cardiovascular diseases (cvds). Available at https://www.who.int/en/news-room/fact-sheets/detail/cardiovascular-diseases-(cvds), june 2021.

[27] Tasos C. Papanastasiou, Georgios C. Georgiou, and Andreas N. Alexandrou. *Viscous Fluid Flow*. CRC Press, 1999.

[28] Gianni Pedrizzetti. *Fluid Mechanics for Cardiovascular Engineering*. Springer, 2022.

[29] Gianni Pedrizzetti and Karl Perktold. *Cardiovascular Fluid Mechanics*. Springer-Verlag Wien, 2003.

[30] MD Peter WF Wilson. Overview of established risk factors for cardiovascular disease. Available at https://www.uptodate.com/contents/overview-of-established-risk-factors-for-cardiovascular-disease/print?search=cardiovascular, january 2022.

[31] N. Pinho, Catarina F. Castro, Carlos Conceição António, Nuno Bettencourt, Luísa Sousa, and Sónia Isabel Silva Pinto. Correlation between geometric parameters of the left coronary artery and hemodynamic descriptors of atherosclerosis: Fsi and statistical study. *Medical & Biological Engineering & Computing*, 57:715–729, 2018.

[32] S.I.S. Pinto, E. Romano, C.C. António, L.C. Sousa, and C.F. Castro. The impact of non-linear viscoelastic property of blood in right coronary arteries hemodynamics — a numerical implementation. *International Journal of Non-Linear Mechanics*, 123:103477, 2020.

[33] Tamilselvi Ramanathan and Henry Skinner. Coronary blood flow. *Continuing Education in Anaesthesia Critical Care Pain*, pages 61–64, april 2005.

[34] Kiichi Sagawa, Reidar K. Lie, and Jochen Schaefer. Translation of otto frank's paper "die grundform des arteriellen pulses" zeitschrift für biologie 37: 483–526 (1899). *Journal of Molecular and Cellular Cardiology*, 22(3):253–254, 1990.

[35] Bernd Saugel, Karim Kouz, Thomas W.L. Scheeren, Gillis Greiwe, Phillip Hoppe, Stefano Romagnoli, and Daniel de Backer. Cardiac output estimation using pulse wave analysis—physiology, algorithms, and technologies: a narrative review. *British Journal of Anaesthesia*, 126(1):67–76, 2021.

[36] Nhan Phan Thien and Roger I. Tanner. A new constitutive equation derived from network theory. *Journal of Non-Newtonian Fluid Mechanics*, 2(4):353–365, 1977.

[37] Stephanie M. Toy, Julius Melbin, and Abraham Noordergraaf. Reduced models of arterial systems. *IEEE Transactions on Biomedical Engineering*, BME-32:174–176, 1985.

[38] I.E. Vignon-Clementel, C.A. Figueroa, K.E. Jansen, and C.A. Taylor. Outflow boundary conditions for 3d simulations of non-periodic blood flow and pressure fields in deformable arteries. *Computer Methods in Biomechanics and Biomedical Engineering*, 13(5):625–640, 2010.

[39] A.J. Weinhaus and K.P. Roberts. *Handbook of Cardiac Anatomy, Physiology, and Devices*. Humana Press, 2005.

[40] Nicolaas Westerhof, Jan-Willem Lankhaar, and Berend Westerhof. The arterial windkessel. *Medical biological engineering computing*, 47:131–41, 07 2008.

[41] Frank M. White. *Fluid Mechanics, Fourth Edition*. McGraw-Hill, 1999.

[42] Peter L. Williams and Roger Warwick. *Gray's Anatomy, Portuguese Version*. Guanabara Koogan, 1995.

[43] J.R. Womersley. Method for the calculation of velocity, rate of flow and viscous drag in arteries when the pressure gradient is known. *The Journal of Physiology*, pages 553–563, march 1955.

[44] M. Zamir. *The Physics of Coronary Blood Flow*. Springer, 2005.

[45] Étienne Puymirat et al. Fractional flow reserve: Concepts, applications and use in france in 2010. *Archives of Cardiovascular Diseases*, pages 615–622, november-december 2010.